Advances in Water Resources 33 (2010) 762–781

Contents lists available at ScienceDirect

Advances in Water Resources

journal homepage: www.elsevier.com/ locate/advwatres

Modelling biofilm growth in the presence of carbon dioxide and water flow in the subsurface

Anozie Ebigbo [a,*], Rainer Helmig [a], Alfred B. Cunningham [b], Holger Class [a], Robin Gerlach [b]

[a] Department of Hydromechanics and Modelling of Hydrosystems, Universität Stuttgart, Pfaffenwaldring 61, 70569 Stuttgart, Germany
[b] Center for Biofilm Engineering, Montana State University, Bozeman, MT 59717, USA

ARTICLE INFO

Article history:
Received 16 October 2009
Received in revised form 31 March 2010
Accepted 10 April 2010
Available online 18 April 2010

Keywords:
Biofilm growth
CO_2 storage
Leakage

ABSTRACT

The concentration of greenhouse gases – particularly carbon dioxide (CO_2) – in the atmosphere has been on the rise in the past decades. One of the methods which have been proposed to help reduce anthropogenic CO_2 emissions is the capture of $CO_2$from large, stationary point sources and storage in deep geological formations. The caprock is an impermeable geological layer which prevents the leakage of stored CO_2, and its integrity is of utmost importance for storage security. Due to the high pressure build-up during injection, the caprock in the vicinity of the well is particularly at risk of fracturing. Biofilms could be used as biobarriers which help prevent the leakage of CO_2 through the caprock in injection well vicinity by blocking leakage pathways. The biofilm could also protect well cement from corrosion by CO_2-rich brine.

The goal of this paper is to develop and test a numerical model which is capable of simulating the development of a biofilm in a CO_2 storage reservoir. This involves the description of the growth of the biofilm, flow and transport in the geological formation, and the interaction between the biofilm and the flow processes. Important processes which are accounted for in the model include the effect of biofilm growth on the permeability of the formation, the hazardous effect of supercritical CO_2 on suspended and attached bacteria, attachment and detachment of biomass, and two-phase fluid flow processes. The model is tested by comparing simulation results to experimental data.

© 2010 Elsevier Ltd. All rights reserved.

1. Introduction

The fundamental motive of this work is the incorporation of concepts and equations describing microbial biofilm processes into a simulator, which models two-phase fluid flow through porous media, with the purpose of examining the interactions between the fluid phases flowing through the porous medium, dissolved constituents, and microorganisms—either attached or suspended in a fluid. Many modelling studies exist in the literature which attempt to model biofilms in porous media. However most account foronly one fluid phase (i.e., saturated flow), e.g., [5–8,16,20,22,24,32,49,51,53]. Few studies describe models capable of simulating a system consisting of two fluid phases flowing through a porous medium containing a biofilm or suspended bacteria, e.g., [17,28,31,41–43,59,63]. The work presented here models this system using a dual-continuum concept – assuming that the biofilm phase can contribute to flow – and empirically accounts for the effect of the presence of the two fluid phases on bacterial growth and decay. Many existing models focus on such applications as microbially enhanced oil recovery and bioremediation. The present work focuses on the application of the model to the mitigation of leakage from a geologic carbon dioxide (CO_2) storage reservoir.

The effects of global warming on the environment are diverse and often beyond human control. Anthropogenic emissions of greenhouse gases, particularly CO_2, have been made primarily responsible for the temperature increase. The use of more efficient technology and regenerative energy sources are ways of reducing emissions. Additionally, CO_2 could be captured from flue gases of power plants and stored in geological formations. Suitable storage formations should have the capacity to accommodate large amounts of CO_2 and guarantee a high storage security. Substantial leakage of CO_2 from a reservoir would render any storage operation useless and could even compromise groundwater resources and human life. Hence, the proper assessment of the risk of CO_2 leakage from a potential storage reservoir is a key issue that needs to be addressed (see [25,35]). Minimising the risk of leakage could include sealing potential leakage pathways. [12] propose the use of microbial biofilms to plug such pathways. Experiments show that biofilms can significantly increase the resistance of a porous medium to flow (e.g., [30,50,58]). Setting up such a hydraulic barrier in the subsurface requires proper judgment of relevant flow, transport, and microbial processes. Numerical models are indispensable for the study of these processes and their interactions with each other.

In the following, the topics of microbial biofilms and CO_2 storage in geological formations are discussed in brief.

* Corresponding author. Tel: +49 711 685 69161; fax: +49 711 685 60430.
E-mail address: anozie.ebigbo@iws.uni-stuttgart.de (A. Ebigbo).

0309-1708/$ – see front matter © 2010 Elsevier Ltd. All rights reserved.
doi:10.1016/j.advwatres.2010.04.004

1.1. Microbial biofilms

Bacteria and other microorganisms can exist as suspended or floating cells in a bulk fluid — planktonic. However, in natural environments, microbial cells tend to be sessile, i.e., attached to a solid surface. Attached cells are often embedded in a matrix of extracellular polymeric substances (EPS) which protects the bacterial cells from environmentally harsh conditions. This assembly of EPS and microbial cells attached to a solid surface (substratum) is referred to as a biofilm.

The structure of biofilms is very heterogeneous. Cells within a biofilm tend to form clusters leaving open spaces within the structure. Biofilms in porous media grow on the surface of the solid matrix, occupying pore space and obstructing fluid flow through pore throats. Hence, the accumulation of biomass in a porous medium can lead to changes in the hydraulic properties (porosity, permeability) of the medium. This and the ability of attached bacteria to degrade certain compounds give rise to a range of applications in which biofilm-affected porous media are used as biofilters and biobarriers [11,30,40,64].

1.2. CO_2 storage in geological formations

Geological sites suitable for subsurface CO_2 storage include deep saline aquifers, depleted oil and gas reservoirs, and coal seams. The CO_2 is injected into geological formations at great depths (>800 m). Due to the high pressures and temperatures at such depths, the injected CO_2 would be either a liquid or a supercritical fluid. The injected CO_2, which is lighter and less viscous than the formation water (brine), would form a separate phase. The resulting CO_2 plume would, driven by the injection pressure, move radially into the formation. Due to buoyancy, it would also be driven upwards. An impermeable geological layer (caprock) is necessary to prevent the buoyant CO_2 plume from rising to the surface (see Fig. 1). Fractures in the caprock or leaky wells can act as leakage pathways for the injected CO_2 [14,34,38]. As an example, the reinjection of oily water into the Tordis subsea field in 2008 led to significant leakage of oil-contaminated formation water through fractures in the caprock into the North Sea[1].

Wells used for the injection of CO_2 into geological formations need to be able to withstand the high pressure build-up during injection and corrosion by CO_2-rich brine. The pressure increase due to injection is highest in the vicinity of the injection well. Its magnitude is dependent, among others, on the viscosities of CO_2 and brine, and on relative permeability effects. Due to low CO_2 saturations during the initial injection phase, the pressure build-up can be quite significant. This can cause fractures in the caprock. If the gas pressure exceeds the capillary entry pressure of the caprock, the CO_2 can penetrate the caprock. The injection rate can be regulated to prevent pressures that exceed some preestimated critical pressure. Injectionwell integrity can be undermined by corrosive CO_2-water mixtures causing degradation of well cement.

Mitchell et al. [30] have suggested the use of engineered biofilms to plug CO_2 leakage pathways. This would entail injecting microbial cells and nutrients at the caprock–aquifer interface before the injection of CO_2 into the formation with the intention of growing a biofilm which would plug potential leakage pathways. Cunningham et al. [12] also propose the use of biofilms which are capable of actively precipitating calcium carbonate ($CaCO_3$) minerals, in which case, a medium containing calcium ions would be injected after the formation of the biofilm.

[1] See Statoil Annual Report 2008. <http://www.statoil.com/AnnualReport2008/en/Sustainability/Environment/Pages/5-3-1-4_InjectedWaterLeakAtTordisAndVisund.aspx>. Retrieved, April 15, 2010.

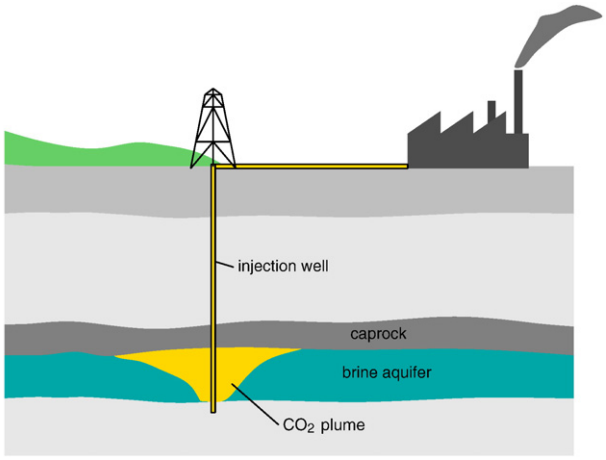


Fig. 1. Concept of CO_2 storage in a brine aquifer.

1.3. Objective

The objective of this work is the *development of a numerical model which can aid in assessing the feasibility of the use of biobarriers to increase CO_2 storage security*. To this end, a model is described in Section **2** and tested against experiments in Section 3. Finally, it is applied to a field-scale test case in Section 2 in which leakage through the caprock of a formation is mitigated using biofilms.

2. Physical and mathematical model

This section focuses on the description of a conceptual model capable of representing the relevant processes involved in a system which consists of a natural porous medium, two fluid phases (water and CO_2), and a biofilm (see Fig. 2). Such a system is typically characterised by a hierarchy of length scales (e.g., [19,23,60]). On the *cell scale*(characteristic length ~1 μm), individual bacterial cells and EPS, which make up the biofilm, can be identified. These cells form clusters held together by EPS. Given that the clusters are sufficiently large compared to the individual cells, one can treat these as a continuum, giving rise to the *biofilm scale*. The void spaces within a biofilm can serve as channels (characteristic pore diameter ~10 μm) for advective flow (see [13,48]). If the thickness of the biofilm phase is sufficiently large compared to the size of the channels/voids within the biofilm, the flow processes through the biofilm may be described on the average with effective properties. These channels contribute to the overall flow of fluids through the porous medium/rock (characteristic pore diameter ~100 μm). Obviously, flow processes as well as concentrations of solutes and bacterial cells within and outside the biofilm may differ significantly leading to strong gradients across the biofilm–fluid interface.

On the *pore scale* (microscale), the grains of the porous medium, which make up the solid phase, are impermeable. The biofilm is attached to the solid phase and occupies part of the porous medium's void space. The rest of this space is occupied by the fluids.

Pore-scale flow processes can be averaged (e.g., [19,56]) on a larger scale (Darcy scale) giving rise to effective, macroscale parameters and equations which describe the porous medium and the interaction between the fluid, biofilm, and solid phases. Depending on the application in mind, one may or may not explicitly account for the flow and transport processes in the biofilm on the macroscale. In this work, the characteristic flow rates through the open pores of the porous medium and through the biofilm have direct consequences for the permeability changes caused by biofilm growth, the transport of nutrients, and the potential presence of CO_2 inside the biofilm. These are important factors which are difficult to describe properly without explicitly accounting for flow through the biofilm. Hence, a

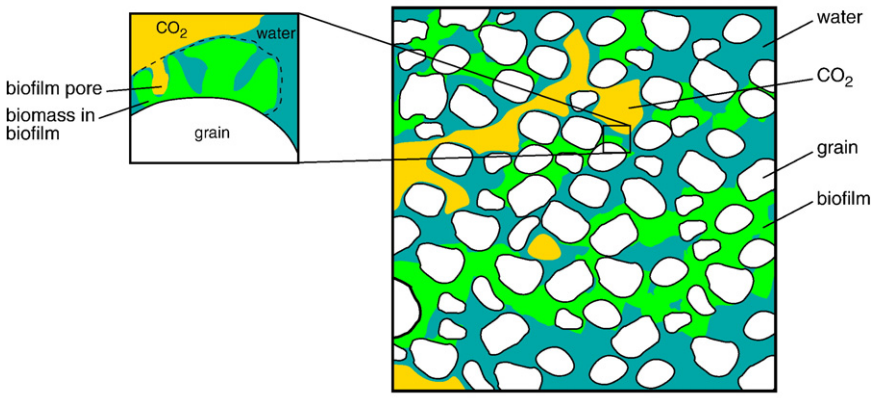


Fig. 2. For flow and transport processes involving two fluid phases and a biofilm within a porous medium, various characteristic length scales can be identified. The figure shows a conceptual model of how the fluids (water and CO_2) may be distributed within the porous medium (on the pore scale, characteristic pore diameter ~100 μm) and within the biofilm (on the biofilm scale, characteristic pore diameter ~10 μm).

distinction is made here between two different components of the flow processes — fast flow through the open pores of the porous medium and slow flow through the biofilm within the porous medium. This can be seen in analogy to the dual-continuum concepts of fractured porous media. Two continua can be defined as shown in Fig. 3. Continuum *P* accounts for flow through the open pores and Continuum *F* for flow through the biofilm embedded in the porous medium. Mass balance equations can be set up for each continuum and the variables of both continua linked by mass transfer terms.

Definitions of the volume fractions which describe the proportions of each component of the system (see Fig. 4) are given in the following.

- The original porosity ϕ_0 of the porous medium is defined as the pore volume of the porous medium unaffected by the biofilm within a representative elementary volume (REV) divided by the bulk volume of the REV.
- The porosity ϕ_p of Continuum *P* is defined as the pore volume of the porous medium excluding biofilm pores divided by the bulk volume of the REV.
- The porosity ϕ_f of Continuum *F* is defined as the volume of pores within the biofilm divided by the bulk volume of the REV.
- The biofilm porosity ε is defined as the volume of pores within the biofilm divided by the total biofilm volume. It is related to ϕ_f and ϕ_p in the following way:

$$\varepsilon = \frac{\phi_f}{\phi_0 - \phi_p}. \tag{1}$$

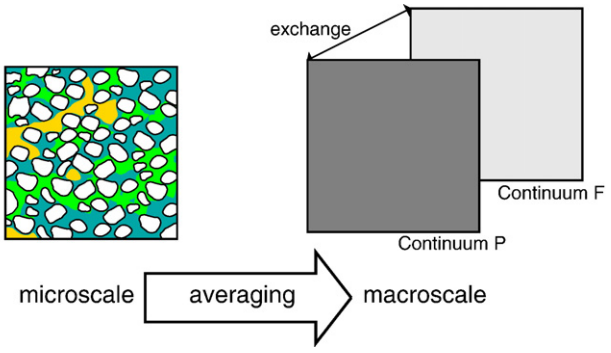


Fig. 3. Schematic diagram of dual-continuum concept applied to biofilm-affected porous media. Continuum *P* accounts for flow through the pores of the porous medium and Continuum *F* for flow through the biofilm. Note that the model presented in this article is defined entirely on the macroscale, and no upscaling techniques have been applied for its derivation.

2.1. Mass conservation equations

In the following, continuity equations for the fluid phases, biomass, and a substrate are given. Note that the formulation of these equations in this work is heuristic.

2.1.1. Conservation of mass of water and CO_2

The mass balance equation for each phase α within the continuum κ reads

$$\frac{\partial\left(\phi_\kappa S_{\alpha,\kappa}\varrho_{\alpha,\kappa}\right)}{\partial t} + \nabla\cdot\left(\varrho_{\alpha,\kappa}\mathbf{v}_{\alpha,\kappa}\right) = q_{\alpha,\kappa} + e_{\alpha,\kappa}; \quad \alpha\in\{w,n\}, \quad \kappa\in\{p,f\}, \tag{2}$$

where $S_{\alpha,\kappa}$ and $\varrho_{\alpha,\kappa}$ are saturation and density, respectively. Water is the wetting phase *w*, and CO_2 is the non-wetting phase *n*. Sources and sinks are represented by $q_{\alpha,\kappa}$, and $e_{\alpha,\kappa}$ accounts for the exchange of mass between two continua. Both continua are treated as porous media in which the Darcy equation is valid (conditions for validity of the Darcy equation, e.g., low Reynolds numbers, can be found, e.g., in [21]). The Darcy velocities $\mathbf{v}_{\alpha,\kappa}$ are calculated as

$$\mathbf{v}_{\alpha,\kappa} = -\frac{k_{r\alpha,\kappa}}{\mu_{\alpha,\kappa}} K_\kappa \left(\nabla p_{\alpha,\kappa} - \varrho_{\alpha,\kappa}\mathbf{g}\right), \tag{3}$$

where $k_{r\alpha,\kappa}$ is relative permeability, $\mu_{\alpha,\kappa}$ is dynamic viscosity, $p_{\alpha,\kappa}$ is pressure, K_κ is intrinsic permeability, and $\mathbf{g}$ is the vector of acceleration due to gravity. The dissolution of CO_2 in water and water in CO_2 is neglected. Dissolved CO_2 may have a detrimental effect on bacterial cells. Due to this simplification, such an effect would not be explicitly accounted for by the model. Note that Eq. (3) is

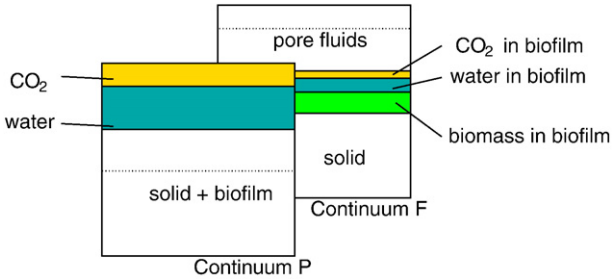


Fig. 4. Illustration of the various components of the system, their volumetric proportions (exemplarily) as needed for the calculation of volume fractions, and their relevance in each continuum.

supplemented by the equations and constitutive relationships given below.

$$\begin{aligned} 1 &= S_{w,\kappa} + S_{n,\kappa} \\ p_{c,\kappa}\left(S_{w,\kappa}\right) &= p_{n,\kappa} - p_{w,\kappa} \\ k_{r\alpha,\kappa} &= k_{r\alpha,\kappa}\left(S_{w,\kappa}\right) \end{aligned} \tag{4}$$

Capillary pressure $p_{c,\kappa}$ and relative permeabilities are calculated using Brooks–Corey relationships (e.g., [10]). The Brooks–Corey formulation of the capillary pressure–saturation relationship is advantageous here since it explicitly accounts for entry pressure. It is worth noting that capillary pressure as used here is a Darcy-scale quantity (see [27]). The above equations assume that each continuum can be characterised with a set of parameters such as porosity ϕ_κ, entry pressure $p_{d,\kappa}$, and pore-size distribution index λ_κ as can be seen in Eq. (15).

2.1.2. Conservation of biomass

Conservation equations for the biomass in the system also need to be formulated. Again, this is done for each continuum. At this point, the following assumptions are made.

- In Continuum *P*, biomass exists only as suspended cells within the water phase and can be accounted for with a concentration C_w^b [kg/m^3]. Biomass in the CO_2 phase is neglected since supercritical CO_2 is a biocide [29].
- In Continuum *F*, biomass exists only in the biofilm, i.e., attached. The properties of the biofilm, namely, biofilm density ϱ_b and biofilm porosity ε are taken to be constant. See Eq. (1) for the definition of ε. Here, biofilm density ϱ_b is defined as the amount of biomass per volume of biofilm *including* the biofilm pore volume.

Thus, the conservation equation for biomass in Continuum *P* (suspended) reads

$$\frac{\partial\left(\phi_p C_w^b S_{w,p}\right)}{\partial t} + \nabla\cdot\left(C_w^b \mathbf{v}_{w,p}\right) - \nabla\cdot\left(D_p^b \nabla C_w^b\right) = q_p^b + e_p^b. \tag{5}$$

C_w^b is the concentration of biomass in the water phase, q_p^b is a source/sink term with which biomass growth and decay can be accounted for, and e_p^b is an exchange term. The coefficient of molecular diffusion of suspended biomass in the water phase D_p^b within a porous medium varies with porosity and saturation (e.g., [2]); $D_p^b = \hat{D}_p^b \phi_p S_{w,p}$. $\hat{D}_p^b$ is a constant diffusion coefficient. Here, the effects of changes in tortuosity with respect to saturation have been neglected. Mechanical dispersion is not included, and this may lead to errors in the calculation of the diffusive fluxes. The accuracy of the calculated diffusive fluxes is further reduced by numerical dispersion which may depend on the spatial and temporal resolution of a given simulation and on the velocity of the fluid.

In Continuum *F*, biomass is immobile, therefore, the mass balance equation consists of only storage and source/sink terms.

$$\frac{\partial\left(\left[\phi_0 - \phi_p\right]\varrho_b\right)}{\partial t} = q_f^b + e_f^b \tag{6}$$

Inserting Eq. (1), yields

$$\left(\frac{\varrho_b}{\varepsilon}\right)\frac{\partial \phi_f}{\partial t} = q_f^b + e_f^b, \tag{7}$$

ε and ϱ_b have been pulled out of the differential because they are taken to be constant. Note that

$$e_f^b = -e_p^b. \tag{8}$$

2.1.3. Conservation of mass of growth-limiting substrate

Bacterial cells, both attached and floating, need the appropriate pH, temperature, salinity etc. to survive. They also need energy, carbon, and an electron acceptor source for metabolism and reproduction. However, it is assumed here that the availability of one substrate limits bacterial growth. Therefore, the growth of biomass is essentially a function of the concentration of this substrate in water. The validity of this assumption depends strongly on the specific conditions in the aquifer and on the characteristics of the bacteria. For example, it could well be that soluble electron acceptors (e.g., oxygen) get used up quickly at which point the available electron acceptors in the aquifer exist as solid minerals which are only available to the biofilm and not to the planktonic cells. In this case, biomass growth would only be possible by the biofilm, and that would violate the assumption made above. However, if a soluble electron acceptor is injected with the substrate, such a situation would not arise.

A mass balance of the growth-limiting substrate gives

$$\frac{\partial\left(\phi_\kappa S_{w,\kappa} C_{w,\kappa}^s\right)}{\partial t} + \nabla\cdot\left(C_{w,\kappa}^s \mathbf{v}_{w,\kappa}\right) - \nabla\cdot\left(D_\kappa^s \nabla C_{w,\kappa}^s\right) = q_{w,\kappa}^s + e_{w,\kappa}^s. \tag{9}$$

D_κ^s is a porosity-dependent diffusion coefficient: $D_\kappa^s = \hat{D}_\kappa^s \phi_\kappa S_{w,\kappa}$, where $\hat{D}_\kappa^s$ is a constant diffusion coefficient.

In Eq. (9), the dissolution of substrate in CO_2 has been neglected. Depending on the substrate, its solubility in supercritical CO_2 may not be negligible. In that case, a balance equation which accounts for the transfer of substrate between the phases would be necessary.

2.2. Simplifying assumptions and exchange terms

A total of eight conservation equations, four in each continuum, were set up in Section 2.1. Some of the equations can be linked by exchange terms which describe the flow of mass from one continuum to the other as a function of a difference in potential. Some assumptions can also be made which significantly reduce the complexity, while bearing in mind the consequences this has on accuracy.

2.2.1. Fluid exchange

Mass exchange of water and CO_2 between the continua can be achieved with an exchange term e_α [kg/(m^{3}s)] which is a function of the pressure difference between the two continua.

$$\begin{aligned} &e_\alpha = a_\alpha\left(p_{\alpha,p} - p_{\alpha,f}\right), \\ &\text{with } e_\alpha = -e_{\alpha,p} = e_{\alpha,f}. \end{aligned} \tag{10}$$

a_α is a parameter which describes the rate at which the exchange takes place.

For simplicity and as a first step in the development of this model, the pressures in the two continua are assumed to be equal. The consequence of this simplification is that fluid exchange takes place instantaneously, and it is not possible to quantify the exchange rate which may be important for the determination of solute exchange. In this work, solute exchange is assumed to be driven primarily by concentration gradients (see Section 2.2.5). The topic of further work has to be the investigation of the importance of solute exchange due to advection and the implementation into the model.

As stated above, it is assumed that for each local REV

$$p_{\alpha,p} = p_{\alpha,f} = p_\alpha. \tag{11}$$

Since fluid properties depend on pressure, the following expressions are direct consequences of Eq. (11).

$$\begin{aligned} \varrho_{\alpha,p} &= \varrho_{\alpha,f} = \varrho_\alpha \\ \mu_{\alpha,p} &= \mu_{\alpha,f} = \mu_\alpha \end{aligned} \tag{12}$$

The capillary pressures at the interface between the two continua have to be the same.

$$p_{c,p} = p_{c,f} = p_c \tag{13}$$

Note that no wettability changes will be accounted for in this work, i.e., both the porous medium and the biofilm are taken to be hydrophilic media. Capillary pressure p_c can be expressed as a function of either of the effective saturations $S_{e,p}$ or $S_{e,f}$. Thus, $S_{e,p}$ and $S_{e,f}$ are not independent. Note that

$$S_{e,\kappa} = \frac{S_{w,\kappa} - S_{wr,\kappa}}{1 - S_{wr,\kappa}} \tag{14}$$

If one of the two is known (e.g., $S_{e,p}$), the other can be calculated as a function of p_c in the following manner (see also Fig. 5).

$$\begin{aligned} p_c &= p_{d,p} S_{e,p}^{-\frac{1}{\lambda_p}}, \\ S_{e,f} &= \left(\frac{p_{d,f}}{p_c}\right)^{\lambda_f} \quad \text{if } p_c > p_{d,f}, \\ S_{e,f} &= 1 \qquad \text{otherwise}. \end{aligned} \tag{15}$$

This means that the distribution of the two fluids within the two continua is determined by capillary forces. It is assumed that $p_{d,f} > p_{d,p}$, so that the non-wetting phase invades Continuum P first before Continuum F, and for a given range of CO_2 saturations in Continuum P, no CO_2 is present in Continuum F. This results from the assumption that the largest pores of the porous medium are larger than those of the biofilm.

Eq. (3) for the water phase becomes

$$\frac{\partial\left(\phi_p S_{w,p} \varrho_w\right)}{\partial t} + \nabla\cdot\left(\varrho_w \mathbf{v}_{w,p}\right) = q_{w,p} - e_\alpha \tag{16}$$

and

$$\frac{\partial\left(\phi_f S_{w,f} \varrho_w\right)}{\partial t} + \nabla\cdot\left(\varrho_w \mathbf{v}_{w,f}\right) = q_{w,f} + e_\alpha. \tag{17}$$

Adding Eqs. (16) and (17), gives

$$\frac{\partial\left(\left[\phi_p S_{w,p} + \phi_f S_{w,f}\right]\varrho_w\right)}{\partial t} + \nabla\cdot\left(\varrho_w\left[\mathbf{v}_{w,p} + \mathbf{v}_{w,f}\right]\right) = q_w, \tag{18}$$

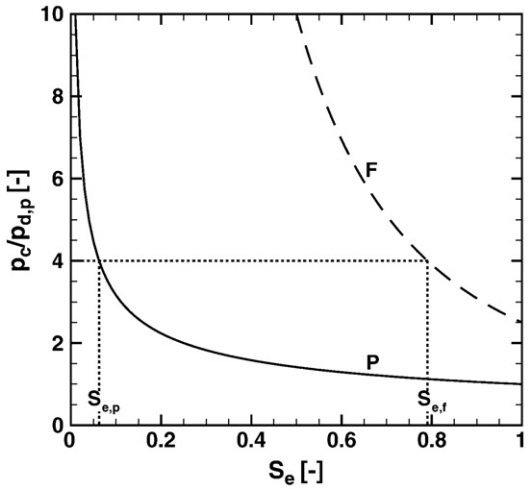


Fig. 5. $S_{e,p}$ and $S_{e,f}$ resulting from one p_c-value. $\lambda_p = 2$, $\lambda_f = \frac{1}{2}$, $p_{d,f} = 2.5 \cdot p_{d,p}$.

where $q_w = q_{w,p} + q_{w,f}$. Similar reformulations can be done for the CO_2 phase.

$$\frac{\partial\left(\left[\phi_p S_{n,p} + \phi_f S_{n,f}\right]\varrho_n\right)}{\partial t} + \nabla\cdot\left(\varrho_n\left[\mathbf{v}_{n,p} + \mathbf{v}_{n,f}\right]\right) = q_n \tag{19}$$

2.2.2. Biomass growth and decay

The terms q_f^b and q_p^b, from Eqs. (5) and (7), comprise biomass growth $r_{g,\kappa}$, biomass decay $r_{b,\kappa}$, and external sources or sinks $\hat{q}_\kappa^b$.

$$q_\kappa^b = r_{g,\kappa} - r_{b,\kappa} + \hat{q}_\kappa^b \tag{20}$$

The growth of biomass $r_{g,\kappa}$ is a function of the biomass concentration or density and a growth rate μ_κ.

$$\begin{aligned} r_{g,p} &= \mu_p \phi_p S_{w,p} C_w^b \\ r_{g,f} &= \mu_f\left(\phi_f / \varepsilon\right)\varrho_b \end{aligned} \tag{21}$$

The growth rate μ_κ depends on the concentration of the growth-limiting substrate and is traditionally modelled with Monod kinetics.

$$\mu_\kappa = k_\mu Y \frac{C_{w,\kappa}^s}{K_s + C_{w,\kappa}^s} \tag{22}$$

k_μ is the maximum substrate utilisation rate, and Y is the yield coefficient which accounts for the fraction of substrate actually used for growth. A great deal of the utilised substrate goes into *cell maintenance*. Notice that both k_μ and Y have been assumed to be the same for both continua, i.e., for both planktonic and sessile cells. A review by [55] finds no conclusive evidence that the attachment of bacterial cells to solid surfaces directly affects metabolism (see also [7]). K_s is the Monod half-saturation coefficient. It is the value of $C_{w,\kappa}^s$ at which $\mu_\kappa = k_\mu Y/2$. These three parameters are species-specific.

Similar functions are used for biomass decay, $r_{b,\kappa}$.

$$\begin{aligned} r_{b,p} &= b_p \phi_p S_{w,p} C_w^b \\ r_{b,f} &= b_f\left(\phi_f / \varepsilon\right)\varrho_b \end{aligned} \tag{23}$$

The decay rate b_κ comprises a constant endogenous decay rate b_0 and a death rate $b_{c,\kappa}$ caused by the cells' exposure to toxic supercritical CO_2.

$$b_\kappa = b_0 + b_{c,\kappa} \tag{24}$$

Zhang et al. [65] and Mitchell et al. [29] suggest likely mechanisms involved in cell inactivation by CO_2. On the one hand, low intracellular pH caused by CO_2 dissolution within a cell may disrupt processes essential for cell activity or cause enzyme denaturation. On the other hand, supercritical CO_2, which is a good solvent, can cause the extraction of intracellular material. In experiments conducted by Mitchell et al. [30] to investigate the effect of supercritical CO_2 on bacterial cells, biofilm cells proved to be more resilient than planktonic cells. This was attributed to the interaction of CO_2 molecules with the EPS matrix leading to an immobilisation of the molecules.

$b_{c,\kappa}$ is a lumped parameter accounting for the different mechanisms responsible for the increased biomass decay due to exposure to CO_2. The most obvious macroscale parameter with which this exposure may be quantified is saturation. Hence, $b_{c,\kappa}$ is assumed to be a function of $S_{n,\kappa}$.

$$b_{c,\kappa} = c_c S_{n,\kappa}^{n_c}, \tag{25}$$

where c_c and n_c are empirical values which may depend on the bacterial species and on the properties of the natural porous medium

and biofilm. Note that while $p_c \leq p_{d,f}$, $S_{n,f}=0$ and thus $b_{c,f}=0$. This means that $S_{n,p}$ has to exceed a critical value before CO_2 can invade Continuum F and cause damage to the biofilm. Before this happens, it is assumed that the free-phase CO_2 does not come in contact with the hydrophilic biofilm. In Continuum P, bacterial cells which attach to the CO_2–water interface are assumed to be inactivated immediately and are included in the saturation-dependent decay term. It must be stated that the transport of dissolved CO_2 is not accounted for in the model and is important for the inactivation processes. Even though these processes are well understood for planktonic cells, it is not clear which mechanisms are important in a biofilm. Given further advancement in this field, it is intended that the model be extended to account for the dissolution of CO_2 in water and to include the dependence of $b_{c,\kappa}$ on the concentration of CO_2 in water.

Once biomass decays, it is no longer accounted for in the model. In effect, therefore, decayed biomass simply disappears causing slight changes in pressure. It is assumed here that the process of growth and decay of biofilm occurs much slower than the flow processes which would equilibrate any such changes in pressure.

2.2.3. Biomass exchange

The exchange terms e_p^b and e_f^b from Eqs. (5) and (7), describe the mass transfer between suspended biomass in Continuum P and attached biomass in Continuum F.

$$e^b = e_f^b = -e_p^b = \underbrace{k_a \phi_p S_{w,p} C_w^b}_{r_a} - \underbrace{k_d \left(\phi_f / \varepsilon\right) \varrho_b}_{r_d} \tag{26}$$

r_a is the rate of attachment of suspended biomass to the solid or biofilm, and r_d is the rate at which biomass detaches from the biofilm. k_a and k_d are attachment and detachment functions, respectively. They are an attempt to account for microscale processes leading to either attachment or detachment on the macroscale.

2.2.3.1. Attachment function. There are a number of different processes, occurring simultaneously, responsible for the attachment of microbial cells in a porous medium. See Corapcioglu and Haridas [9] for a description of these processes.

Due to the strong effect large amounts of biofilm within the porous medium would have on the attachment function, it is imperative that the attachment function should account for variations in attachment with changes in the volume fraction of pore space occupied by attached biomass. Thus, the function by Taylor and Jaffé [51] is used in this work.

$$k_a = c_{a,1} + c_{a,2} \phi_f / \varepsilon \tag{27}$$

$c_{a,1}$ and $c_{a,2}$ are empirical parameters.

In two-phase fluid flow, microorganisms also attach to the interface between the two fluids. This is often incorporated in models with an additional attachment term [17,42,43]. The attachment rate at the fluids' interface is then a function of the interfacial area between the two fluids. This interfacial area can be estimated from the pore-size distribution of the porous medium and is a non-linear function of the wetting-phase saturation [4,33]. However, in this work, one of the fluid phases is a biocide which means that cells attached to the fluids' interface are exposed to the toxic fluid. These are then accounted for by decay term $b_{c,p}$ (see Eq. (25)).

2.2.3.2. Detachment function. Detachment processes, relevant to this work, include erosion and sloughing [3]. Rittmann [39] relates detachment to shear stress. In this case, changes in the force exerted on the biofilm (shear stress) are accounted for as well as the reduction in the strength of the biofilm with increasing thickness. Speitel and DiGiano [46] suggest that an additional detachment term be added to that of Rittmann [39]. This is motivated by experimental data suggesting that fast-growing biofilms detach more readily than slow-growing biofilms. This could be as a result of differences in the production rate of EPS compared to cell reproduction. It could also result from an increasingly uneven growth as growth rate increases. Picioreanu et al. [36] could show, using numerical simulations, that differences in shape and structure between fast and slow-growing biofilms is one reason for the differences in susceptibility to shear.

The detachment function given in Eq. (28) is a function of the magnitude of the water-phase pressure gradient $|\nabla p_w|$. It is assumed that the pressure gradient accounts for the shear forces exerted on the biofilm by the water phase. It is also assumed, as discussed above, that a higher growth rate increases biofilm susceptibility to shear. This is accounted for, as suggested by [46], by the term k_d^μ.

$$k_d = \underbrace{c_{d,1}\left(\phi_p S_{w,p} |\nabla p_w|\right)^{n_d}}_{k_d^\tau} + \underbrace{c_{d,2} \mu_f \left(\phi_f / \varepsilon\right) \varrho_b}_{k_d^\mu} \tag{28}$$

$c_{d,1}$, $c_{d,2}$, and n_d are empirical parameters. Assuming the dependence of k_d^τ on the pressure gradient behaves in the same way as its dependence on shear stress, the exponent n_d can be taken from Rittmann [39] to be $n_d = 0.58$. The detachment term k_d^μ is proportional to the rate of biofilm growth. Speitel and DiGiano [46] give values for the proportionality factor $c_{d,2}$ ranging from 0.319 to 0.665 depending, for example, on the substrate. In this work, it is assumed that the proportionality between k_d^μ and growth rate varies with the amount of biofilm in place ϕ_f/ε.

$$c_{d,2} = \tilde{c}_{d,2} \phi_f / \varepsilon \tag{29}$$

The dependence of $c_{d,2}$ on ϕ_f/ε accounts for the increase in variation of the substrate distribution within the biofilm with increase in biofilm thickness resulting in uneven biofilm growth, and hence in greater detachment.

2.2.4. Substrate consumption

Substrate is utilised by biomass in both continua. Therefore, $q_{w,\kappa}^s$ in Eq. (9) is a sink and a function of the bacterial substrate utilisation rates.

$$q_{w,\kappa}^s = -r_{g,\kappa} / Y \tag{30}$$

2.2.5. Substrate exchange

The transfer of substrate between the two continua is accounted for by the term $e_{w,\kappa}^s$ in Eq. (9). It is a function of the difference in substrate concentration in the two continua.

$$e_w^s = -e_{w,p}^s = e_{w,f}^s = a_w^s \left(C_{w,p}^s - C_{w,f}^s\right) \tag{31}$$

The parameter a_w^s describes the rate at which the exchange takes place. This process is often assumed to be mainly diffusive. In dual-continuum models, such exchange terms often take the form (e.g., [18]):

$$e_w^s = D_{eff}^s \frac{\beta}{L^2} \left(C_{w,p}^s - C_{w,f}^s\right) \tag{32}$$

L is a characteristic length over which the concentration difference exists, and β is a dimensionless, geometry-dependent coefficient. These two parameters are difficult to determine and have to be estimated. One way to estimate β/L^2 could be by assuming that mass transfer occurs across the specific surface M of the porous medium over a characteristic length which is equivalent to the characteristic pore radius $d_r/2$. This gives

$$e_w^s = D_{eff}^s \frac{M}{d_r/2} \left(C_{w,p}^s - C_{w,f}^s\right). \tag{33}$$

D^s_{eff} can be interpreted as the effective diffusivity of the solute in the biofilm [47,61].

2.3. Clogging

Many studies have focused on deriving a mathematical expression linking the permeability of a porous medium to its porosity, e.g., Taylor et al. [52], Vandevivere [57], Clemental et al. [6], Seki and Miyazaki [44], Thullner et al. [54]. There are also some studies on the effect of bacterial accumulation on changes in permeability or pore-size distribution in an unsaturated porous medium, e.g., Rockhold et al. [41], Maggi and Porporato [28], Mostafa and Van Geel [31]. In experiments, the effect of biofilm growth on permeability has been shown [11,58]. They generally show a strong initial decrease in intrinsic permeability with decrease in porosity followed by a region in which only minor changes in permeability are observed (see Fig. 6). The shape of the permeability–porosity curve is dependent on both the properties of the porous medium and of the biofilm.

In the model described here, two permeabilities exist. Each continuum is assigned a permeability. With a summation of the individual fluxes within a control volume, it can be shown that for saturated flow and with the assumption made in Section 2.2.1 (equal pressures in both continua), that the total intrinsic permeability K as measured in the experiments (e.g., by [11]) is equivalent to the sum of the permeabilities of the two continua.

$$K = K_p + K_f \tag{34}$$

This means that one can determine the individual permeability–porosity relationships for each continuum and sum them up for comparison with experimental values. Obviously, the permeability of a porous medium with small amounts of biofilm is mainly dependent on K_p, while that of a biofilm-filled porous medium is mainly dependent on K_f. Thus, the following expressions have to be fulfilled.

$$\begin{aligned} &\text{If } \phi_p = \phi_0 \text{ and } K = K_0 \quad \Rightarrow \quad K_p = K_0 \text{ and } K_f = 0, \\ &\text{if } \phi_p = 0 \text{ and } K = K_{\min} \quad \Rightarrow \quad K_p = 0 \text{ and } K_f = K_{\min}. \end{aligned} \tag{35}$$

K_0 is the permeability of the biofilm-free porous medium, while $K_{\min}$ is the permeability of the biofilm-filled porous medium.

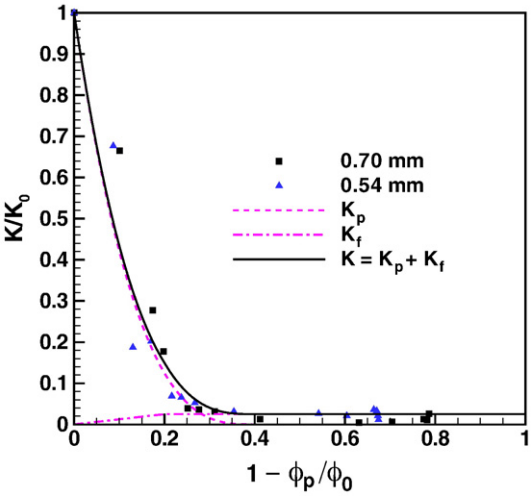


Fig. 6. Mathematical description of permeability decrease with increase in biomass fitted to data from [11] with two sands of different median particle sizes (0.54 mm and 0.70 mm). K as used for the y-axis is the sum of K_p and K_f. The values of the parameters used are $\phi_{p,c}/\phi_0 = 0.6$, $\phi'_{p,c}/\phi_0 = 0.8$, $K_{\min} = 0.025 \cdot K_0$ and $n_k = 3$. K_f is assumed to increase linearly from zero with decreasing ϕ_p until $\phi'_{p,c}$ at which point $K_f = K_{\min}$.

The permeability of Continuum P can be described using the expression given by Xu et al. [62].

$$\begin{aligned} &K_p / K_0 = \left(\frac{\phi_p - \phi_{p,c}}{\phi_0 - \phi_{p,c}}\right)^{n_k} \quad \text{if } \phi_p > \phi_{p,c}, \\ &K_p = 0 \qquad\qquad\qquad\qquad \text{otherwise}. \end{aligned} \tag{36}$$

$\phi_{p,c}$ is the porosity at which $K_p = 0$, and n_k is an empirical parameter which is strongly dependent on the geometry of the porous medium. From the experimental data in Fig. 6, one can determine values of $K_{\min}$ for the various sands, and since these values are relatively constant, it seems appropriate to assign K_f the constant value $K_{\min}$. However, at $\phi_p = \phi_0$, K_f has to be zero. Thus, one could think of a $\phi_p = \phi'_{p,c}$ for which the following holds.

$$\begin{aligned} &K_f = K_{\min} \qquad \text{if } \phi_p \le \phi'_{p,c}, \\ &K_f < K_{\min} \qquad \text{otherwise}. \end{aligned} \tag{37}$$

For the region in which $K_f < K_{\min}$, there could be a number of different concepts to describe the behaviour of K_f. However, the concept used is not very important because its contribution to the overall flow process is very small within that region. A simple concept is to have K_f continuously increase from zero to $K_{\min}$ as ϕ_p decreases from ϕ_0 to $\phi'_{p,c}$. The resulting permeability–porosity relationship is shown in Fig. 6.

Vandevivere [57] describes a similar expression for the permeability–porosity relationship. He identifies two clogging mechanisms, and their weighted contributions are summed to get the permeability of the porous medium.

2.3.1. Neglected effects of biofilm growth on porous medium

Biofilm growth in a porous medium would probably also change the pore-size distribution represented in this work by the pore-size distribution index λ. Maggi and Porporato [28] introduces concepts with which one could account for these changes. Such changes in pore-size distribution are not included in the presented model. Also neglected are potential changes in entry pressure due to biofilm growth.

2.4. System of equations

As a summary of Section **2**, the equations which describe the model concept are given in Table 1. The primary variables of the system of equations are $S_{w,p}$, p_n, C^b_w, ϕ_f, $C^s_{w,p}$, and $C^s_{w,f}$.

2.5. Numerical model

The balance equations in Table 1 form a system of strongly coupled, non-linear partial differential equations. The complexity of the system of equations calls for a numerical solution. The numerical model used in this work is implemented within the framework of the multiphase flow simulator MUFTE-UG (Multiphase Flow, Transport, and Energy model on Unstructured Grids). A vertex-centred finite volume method is used for spatial discretisation, while the time discretisation is done with a fully implicit Euler scheme.

3. Attempts at model validation

Two experiments have been chosen from literature which deal with problems relevant to this work and with which the model presented in the previous section will be tested. They include an experiment with water-saturated flow through a biofilm-affected porous medium by Taylor and Jaffé [50] and one by Mitchell et al. [30] which deals with the effect of CO_2 on a biofilm grown in a porous medium. The first experiment focuses particularly on the interaction between fluid flow and biofilm growth, while the second experiment

Table 1
System of equations ($\kappa \in \{p,f\}$, $\alpha \in \{w,n\}$).

	Continuum P		Continuum F
	Mass balance equations		
Water	$\frac{\partial([\phi_p S_{w,p} + \phi_f S_{w,f}]\varrho_w)}{\partial t} + \nabla\cdot(\varrho_w[\mathbf{v}_{w,p} + \mathbf{v}_{w,f}]) = q_w$		
CO_2	$\frac{\partial([\phi_p S_{n,p} + \phi_f S_{n,f}]\varrho_n)}{\partial t} + \nabla\cdot(\varrho_n[\mathbf{v}_{n,p} + \mathbf{v}_{n,f}]) = q_n$		
Biomass	$\frac{\partial(\phi_p C^b_{w,p} S_{w,p})}{\partial t} + \nabla\cdot\left(C^b_w \mathbf{v}_{w,p}\right)$		$\left(\frac{\varrho_b}{\varepsilon}\right)\frac{\partial \phi_f}{\partial t} = q^b_f + e^b$
	$-\nabla\cdot(D^b_p \nabla C^b_w) = q^b_p - e^b$		
Substrate	$\frac{\partial\left(\phi_p S_{w,p} C^s_{w,p}\right)}{\partial t} + \nabla\cdot\left(C^s_{w,p}\mathbf{v}_{w,p}\right)$		$\frac{\partial\left(\phi_f S_{w,f} C^s_{w,f}\right)}{\partial t} + \nabla\cdot\left(C^s_{w,f}\mathbf{v}_{w,f}\right)$
	$-\nabla\cdot(D^s_p \nabla C^s_{w,p}) = q^s_{w,p} - e^s_w$		$-\nabla\cdot(D^s_f \nabla C^s_{w,f}) = q^s_{w,f} + e^s_w$
	Sources and sinks		
Biomass		$q^b_\kappa = r_{g,\kappa} - r_{b,\kappa} + \hat{q}^b_\kappa$	
	$r_{g,p} = \mu_p \phi_p S_{w,p} C^b_w$		$r_{g,f} = \mu_f(\phi_f/\varepsilon)\varrho_b$
		$\mu_\kappa = k_\mu Y \frac{C^s_{w,\kappa}}{K_s + C^s_{w,\kappa}}$	
	$r_{b,p} = b_p \phi_p S_{w,p} C^b_w$		$r_{b,f} = b_f(\phi_f/\varepsilon)\varrho_b$
		$b_\kappa = b_0 + c_c S^{n_c}_{n,\kappa}$	
Substrate		$q^s_{w,\kappa} = -r_{g,\kappa}/Y$	
	Exchange terms		
Biomass		$e^b = r_a - r_d$	
	$r_a = k_a \phi_p S_{w,p} C^b_w$		$r_d = k_d(\phi_f/\varepsilon)\varrho_b$
	$k_a = c_{a,1} + c_{a,2}\phi_f/\varepsilon$		$k_d = c_{d,1}(\phi_p S_{w,p}\lvert\nabla p_w\rvert)^{0.58} + \tilde{c}_{d,2}\mu_f(\phi_f/\varepsilon)^2\varrho_b$
Substrate		$e^s_w = D^s_{eff}\frac{M}{d_r/2}\left(C^s_{w,p} - C^s_{w,f}\right)$	
	Supplementary equations and constitutive relationships		
Volume fractions		$\phi_p + \phi_f/\varepsilon = \phi_0$	
Saturations		$\sum_\alpha S_{\alpha,\kappa} = 1$	
Capillary pressure		$p_c = p_n - p_w$	
	$p_{c,p} = p_{d,p} S^{-1/\lambda_p}_{e,p}$		$p_{c,f} = p_{d,f} S^{-1/\lambda_f}_{e,f}$
		$p_{c,p} = p_{c,f}$	
Intr. perm.	$\frac{K_p}{K_0} = \left(\frac{\phi_p - \phi_{p,c}}{\phi_0 - \phi_{p,c}}\right)^{n_k}$ for $\phi_p > \phi_{p,c}$		$K_f = K_{\min}$ for $\phi_p \le \phi'_{p,c}$
Rel. perms.		$k_{rw,\kappa} = S_{e,\kappa}^{\frac{2+3\lambda_\kappa}{\lambda_\kappa}}$	
		$k_{rn,\kappa} = (1 - S_{e,\kappa})^2\left(1 - S_{e,\kappa}^{\frac{2+\lambda_\kappa}{\lambda_\kappa}}\right)$	
Velocities		$\mathbf{v}_{\alpha,\kappa} = -\frac{k_{r\alpha,\kappa}}{\mu_\alpha} K_\kappa(\nabla p_\alpha - \varrho_\alpha \mathbf{g})$	

focuses on the effect of supercritical CO_2 on the development of a biofilm.

3.1. One-phase flow experiments by taylor and Jaffé [50]

3.1.1. General description

Two columns were packed with sand, and biofilms were grown in these columns over several months under constant flow conditions. The columns were inoculated with methanol-utilising bacteria for a few hours after which a constant methanol concentration was maintained in the influent. Pressure was measured at regular intervals along the column, and thus the permeability changes could be quantified.

3.1.2. Simulation parameters

In Table 2, a list of parameters as used in the experiments by Taylor and Jaffé [50] is given. In Column 1, the flow rate and the influent substrate concentration were reduced after 149 days, whereas only the influent substrate concentration was reduced in Column 2.

Taylor and Jaffé [51] developed a numerical model with which they simulated part of the experiment described above. The parameters used in those simulations are listed in Table 3. The experiments have been simulated with the model developed in Section 2. However, since this is a one-phase flow problem, the mass balance equation for CO_2 is not necessary.

The initial and boundary conditions for the problem are given in Table 4. The domain is discretised with 22 uniform elements, i.e., a discretisation length of 0.0236 m. In Section 2.3, the parameters needed to describe changes in permeability were fitted to data given by Cunningham et al. [11] for sands with median grain sizes of 0.54 mm and 0.70 mm. The permeabilites of these sands were 2.17×10^{-10} m^2

Table 2
Parameters for experiments by [50].

Parameter	Column 1	Column 2
Column length	0.52 m	
Column diameter	0.0508 m	
Sand porosity ϕ_0	0.347	
Sand permeability K_0	2.93×10^{-10} m^2	
Mean grain diameter of sand	0.7 mm	
Specific surface of sand M	4.85×10^{3} m^{-1}	
Temperature	15 °C	
Total operation time	284 days	356 days
For $t \le 149$ days		
Influent substrate concentration	7.20×10^{-3} kg/m^3	5.59×10^{-3} kg/m^3
Flow rate	2.22×10^{-5} m^3/s	7.38×10^{-6} m^3/s
For $t > 149$ days		
Influent substrate concentration	5.20×10^{-3} kg/m^3	4.70×10^{-3} kg/m^3
Flow rate	1.37×10^{-5} m^3/s	7.38×10^{-6} m^3/s

Table 3
Parameters used for simulation in [51].

Parameter	Value	
	Column 1	Column 2
Water viscosity μ_w	1.139×10^{-3} Pa · s	
Maximum substrate utilisation rate k_μ	8.91×10^{-5} s^{-1}	
Monod half-saturation coefficient K_s	7.99×10^{-4} kg/m^3	
Yield coefficient Y	0.0975 kg/kg	
Endogenous decay rate b_0	3.18×10^{-7} s^{-1}	
Biofilm density ϱ_b	3 kg/m^3	2.5 kg/m^3
Attachment rate parameter $c_{a,1}$	7.40×10^{-3}	
Attachment rate parameter $c_{a,2}$	7.88×10^{-2}	

and 3.19×10^{-10} m^2, respectively. These values are very close to those of the sand used by Taylor and Jaffé [50] (mean grain size: 0.70 mm, permeability: 2.93×10^{-10} m^2). Thus, the set of parameters from Section 2.3 shown in Fig. 6 are deemed appropriate for the description of changes in permeability in this experiment. They include $\phi_{p,c}/\phi_0=0.6$, $n_k=3$, and $\phi'_{p,c}/\phi_0=0.8$. However, $K_{\min}$ is assumed to be unknown and will be fitted to the experimental results. The sand used by Taylor and Jaffé [50] had a declared permeability of 2.93×10^{-10} m^2. However, judging from their results, the measured permeabilities of the sands unaffected by biomass was a bit lower than K_0. For this reason, in the simulations, the maximum permeability is taken to be 1.42×10^{-10} m^2.

Other parameters used in the simulation include water density $\varrho_w=1000$ kg/m^3, the diffusion coefficients $\hat{D}^b_p=\hat{D}^s_\kappa=10^{-8}$ m^2/s and the effective diffusion coefficient $D^s_{eff}=\varepsilon\times10^{-9}$ m^2/s. The average pore diameter of the sand is estimated using the empirical relation $d_r=6\phi_0/M$, therefore, $d_r=0.43$ mm. Zhang and Bishop [66] observed variations in biofilm porosity ε ranging from 0.58 to 0.93. Here, ε is assigned a value of 0.8. However, the results of the simulation were not very sensitive to changes in ε. The attachment parameters $c_{a,1}$ and $c_{a,2}$ were fitted in the simulations by Taylor and Jaffé [50] (see Table 2).

A total of three parameters were fitted in the simulation of Column 1 and remained unchanged for Column 2 (see Table 4).

3.1.3. Results

Fig. 7 shows the results of the simulations. The logarithmic reduction of permeability caused by biofilm growth is plotted over distance into the columns. The biofilm grows by utilising the substrate at the inlet causing a decrease in permeability. Since the inflow rate is kept constant, this results in a pressure build-up near the inlet. High pressure gradients cause high biomass detachment from the biofilm. Detached cells get transported downstream, where they reattach. This results in an encroachment of the biofilm into the column, the extent of which is dependent on the inflow rate. The simulated permeability reduction in Column 1 was less than observed in the experiments. In Column 2, the simulated biofilm advanced further into the column than in the experiments. The differences between simulations and experiments may result from shortcomings of the model concept, e.g., the assumption that the biofilm density is constant or the way biofilm decay is treated. Biofilm density may vary with biofilm age and external conditions. This is not accounted for in the model. In the model concept, decay of biomass within the biofilm immediately leads to a reduction of the pore space occupied by the biofilm. In reality, obviously, it may take some amount of time for dead biomass to be removed. However, during the experiments, there were problems with the water source [51], and thus the aim of this comparison is mostly qualitative. Column 1 is affected by biomass throughout the column, whereas the biofilm affects only part of Column 2. This can be seen in both the experimental and the simulated results. The permeability values of both experimental

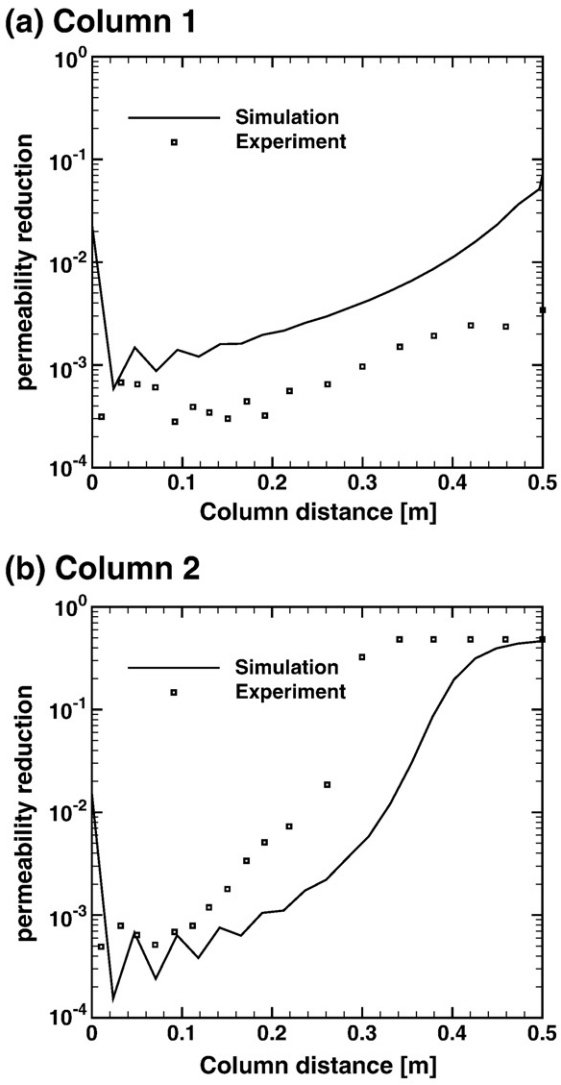


Fig. 7. Comparison of simulated permeability reduction to the experimental results of [50]. The parameters $c_{d,2}$, $\tilde{c}_{d,2}$, and $K_{\min}$ were fitted to the experimental data in Column 1. Possible reasons for the differences between simulations and experimental results are discussed in Section 3.1.3. The mean absolute error in permeability reduction between the simulation and experimental data is 0.8 % in Column 1 and 8 % in Column 2.

Table 4
Initial and boundary conditions, and fitted parameters for simulation of experiments by [50].

Parameter	Value	
	Column 1	Column 2
Initial conditions		
p_w	101325 Pa	
C^b_w	0 kg/m^3	
$C^s_{w,p}$	7.20×10^{-3} kg/m^3	5.59×10^{-3} kg/m^3
$C^s_{w,f}$	0 kg/m^3	
Boundary conditions at $x=0$ m		
Water flux (Neumann)	as given in Table 2	
C^b_w (Dirichlet)	5×10^{-3} kg/m^3 for $t\leq0.212$ days	
(Neumann)	0 kg/m^3 otherwise	
$C^s_{w,p}$ (Dirichlet)	as given in Table 2	
$C^s_{w,f}$ (Neumann)	no flow	
Boundary conditions at $x=0.52$ m		
p_w (Dirichlet)	101325 Pa	
C^b_w (Dirichlet)	0 kg/m^3	
C^s_w (Dirichlet)	0 kg/m^3	
C^s_f (Dirichlet)	0 kg/m^3	
Values of parameters fitted to Column 1		
$c_{d,1}$	2.9×10^{-8}	
$\tilde{c}_{d,2}$	6	
$K_{\min}$	7.33×10^{-20} m^2	

and numerical results near the inlet fluctuate in space. However, these fluctuations are more pronounced in the simulation. This is probably due to the instability of the solution just before or after Continuum P becomes fully clogged ($K_P = 0$). This is however exaggerated by the logarithmic scale.

Concluding, even though the model can qualitatively reproduce and predict the experiments, a quantitative validation was not possible. This calls for further work in this regard as discussed in the Outlook (Section 4).

3.2. Experiments by Mitchell et al. [30] with two phases

3.2.1. General description

These experiments were conducted at high pressure (89 bar) and moderate temperature (32 °C). Two sandstone cores were inoculated with *Shewanella fridgidimarina*. The general strategy in the experiments was to grow a biofilm in the sandstonecore and challenge the biofilm with supercritical CO_2. A saline nutrient medium was injected once or twice a day in pulses lasting between 20 and 200 minutes. With each pulse, the permeability of the core was calculated. The bacteria species *S. fridgidimarina* which was used to inoculate the cores was succeeded by other species originally present in the cores, namely, *Bacillus mojavensis* and *Citrobacter* sp.

3.2.2. Simulation Parameters

The properties of the sandstone cores and the conditions at which the experiments were run are given in Table 5. Also given in the table is the duration of each experiment. The experiments can be divided into different phases depending on the medium. Initially, a saline nutrient medium was injected into the cores at intervals as mentioned in Section 3.2.1 (*growth phase*). In Experiment 1, the growth phase was followed directly by a flooding of the core with CO_2. After the growth phase in Experiment 2, a nutrient-depleted saline solution was injected (*starvation phase*). This was followed by the injection of CO_2, a second starvation phase, and another CO_2 challenge. The different phases of the experiments are summarised in Table 6.

Due to lack of information and for simplicity, the following assumptions will be made in the simulation.

- The periods of flow through the core are neglected. This means that no spatial discretisation is necessary since there are no spatial gradients.
- The effect of suspended biomass is neglected. This implies that the balance equation for biomass in Continuum P is omitted, and there are no attachment or detachment rates.
- During the growth phase, the nutrients needed by the bacterial cells are abundantly available, i.e., the growth rate is independent of the substrate concentration, $\mu_f = k_\mu Y$. The opposite is the case during the starvation phase, $\mu_f = 0$. Therefore, no balance equations for substrate are solved.
- The pore-size distribution and entry pressure of the rock and the biofilm are unknown. The same goes for the amount of CO_2 in the cores during the flooding of the cores with CO_2. Obviously, any fitting of parameters would not be unique. Instead, it will be assumed that λ_κ and $p_{d,\kappa}$ are known, and the CO_2 saturation at the start of the CO_2 challenge is fitted to the experimental data.

With the above assumptions, the mass balance equations from Table 1 simplify to the following.

$$\frac{d\left(\phi_p S_{w,p} + \phi_f S_{w,f}\right)}{dt} = q_w / \varrho_w \tag{38}$$

$$\frac{d\left(\phi_p S_{n,p} + \phi_f S_{n,f}\right)}{dt} = q_n / \varrho_n \tag{39}$$

$$\frac{1}{\phi_f}\frac{d\phi_f}{dt} = \mu_f - b_0 - c_c S_{n,f}^{n_c} \tag{40}$$

The source/sink term q_w is chosen in such a way that the water-phase pressure p_w remains unchanged (accounting for the transfer of intracellular to extracellular water as the biofilm decays), whereas, $q_n = 0$.

In Table 7, the set of parameters used for the simulation of the two experiments are listed. Some of the parameters are estimated based on values from literature. As mentioned above, assumptions have been made for the pore-size distribution indices, entry pressures, and residual saturations of the two phases in the two continua. Three parameters have been fitted to the results of Experiment 2.

The growth phase is initialised, in the experiments, by injecting bacteria suspended in water into the cores and letting the bacteria attach to the rock. In the simulation, the porosity of Continuum F is initialised with $\phi_f = 10^{-4} \cdot \varepsilon$.

3.2.3. Results

The growth of biofilm within the sandstone core causes a permeability reduction. At some point, a minimum permeability value is achieved. In the experiments, this occurs after a small increase in permeability (see Fig. 8). In both experiments, this occurs at about $t \approx 5$ days. The reason for this increase is not clear. Possibly, it occurs

Table 5
Parameters for experiments by [30].

Parameter	Experiment 1	Experiment 2
Column length	0.0508 m	0.1185 m
Sandstone porosity ϕ_0	0.22	
Sandstone permeability K_0	38.96×10^{-15} m^2	47.13×10^{-15} m^2
Pressure	89 bar	
Temperature	32 °C	
Total operation time	20.67 days	34.58 days

Table 6
Duration of the different phases of the experiments by [30].

	Growth	Starvation	CO_2	Starvation	CO_2
	I	II	III	IV	V
Experiment 1	20 days	–	0.67 days	–	–
Experiment 2	12.5 days	15.13 days	4.21 days	0.75 days	2 days

Table 7
Parameters for simulation of experiments by [30].

Parameter	Value	Comment
Growth rate μ_f	4.63×10^{-5} s^{-1}	
Endogenous decay rate b_0	3.18×10^{-7} s^{-1}	From [51]
Decay rate parameter c_c	8.7×10^{-4} s^{-1}	Estimated from [29]
Decay rate parameter n_c	3	Fitted to Experiment 2
Permeability parameter $\phi_{p,c}/\phi_0$	0.35	Fitted to Experiment 2
Permeability parameter n_k	3	
Minimum permeability $K_{\min}$	5.0×10^{-16} m^2	Taken from experimental data
Biofilm porosity ε	0.8	Estimated from [66]
Pore-size distribution indices		
λ_p	2	
λ_f	0.5	
Entry pressures		
$p_{d,p}$	0.1 bar	
$p_{d,f}$	0.25 bar	
Residual saturations		
$S_{wr,p}$	0.15	
$S_{wr,f}$	0.3	
$S_{nr,p}$	0.05	
$S_{nr,f}$	0	
$S_{n,p}$ at start of each CO_2 challenge	0.8	Fitted to Experiment 2

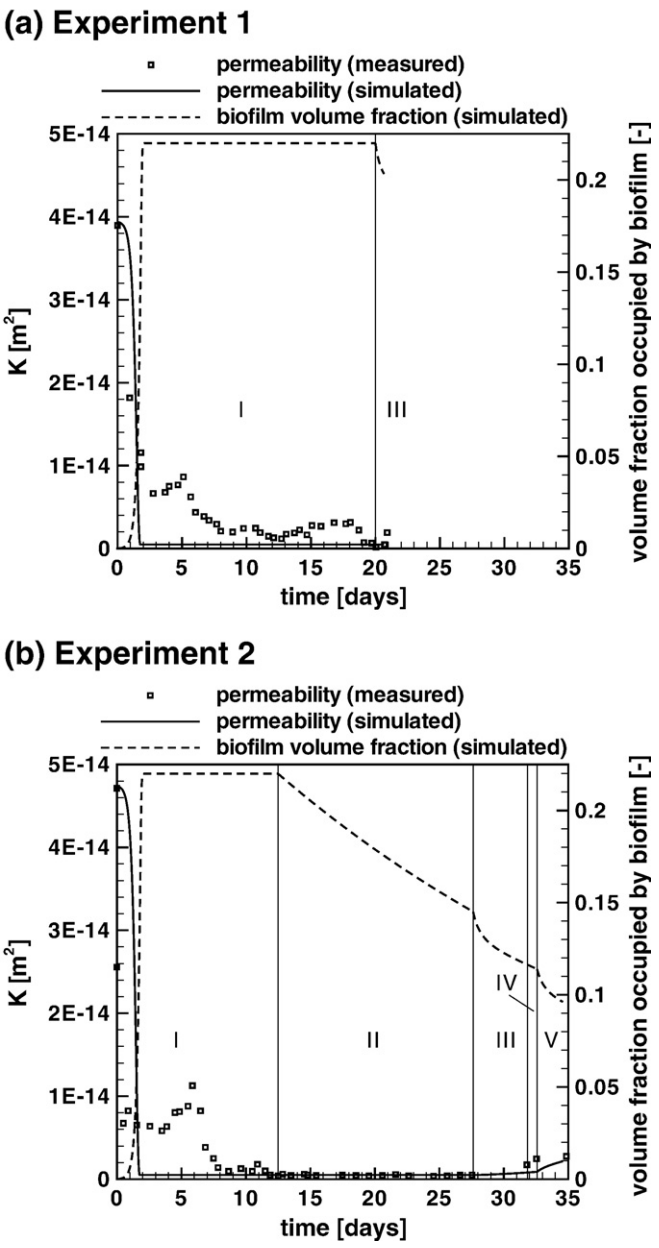


Fig. 8. Comparison of simulated permeability changes to the experimental results of [30]. Three parameters were fitted to Experiment 2 and remained unchanged for the simulation of Experiment 1. The symbols show the measured permeabilities of the sandstone cores in the experiments by [30], and the continuous lines show the permeabilities of the cores in the simulation. The dashed lines show the volume fractions of pore space occupied by attached biomass, which is equivalent to ϕ_f/ε. The experiments are divided into various phases, I, II, III, IV, and V. These are described in Table 6.

due to nutrient limitations at that point. Since no nutrient limitations are accounted for in the simulation, no such increase was modelled. Instead, the permeability decreases monotonously and stagnates at the minimum value of 5×10^{-16} m^2. In Experiment 1, the growth phase is followed directly by a CO_2 challenge in which a slight increase in permeability was observed. The simulation does not show this increase in permeability. However, the effect of the CO_2 on the biofilm can be seen in the sharp decrease in the amount of pore space occupied by the biofilm ϕ_f/ε (see Fig. 8). In Experiment 2, the growth phase is followed by a starvation phase. In the first starvation phase, the permeability remains constantly low. The simulation shows a steady decrease in ϕ_f/ε corresponding to the endogenous decay rate. This first starvation phase is followed by the first CO_2 challenge, a second short starvation phase, and finally the second CO_2 challenge. Both the experiment and simulation show slight increases in permeability in each of the last three phases.

Due the lack of experiments dealing with the processes required for a proper validation of the model, it is not possible at the current stage of research in this field to adequately validate the model. However, the experiments by Mitchell et al. [30] do provide a means of calibration for the parameters which describe the interaction between CO_2 and the biofilm in the model.

3.3. Remarks

The model described in this paper was tested by modelling experiments from literature and comparing the simulations to experimental results. In order to model these experiments numerically, a number of assumptions and simplifications had to be made. Each of the experiments consisted of two runs, each with a different set of parameters and conditions. The model was fitted to one of the two runs and used to predict the results of the other.

The values of the fitted parameters may not be unique. This may question the capability of these comparisons to validate the model. However, it is an excellent way of testing the model and getting a feel for the important parameters and the implications of the modelling assumptions.

4. Model application

In the following, the model presented here will be applied in simulations of processes in the vicinity of a CO_2 injection well.

4.1. General description

The problem set-up is similar to that used in the leakage simulations run by Kopp et al. [26] with which they investigated the thermal effects of leaking CO_2 (see also [37]). In this work, however, the interest is on the caprock and the target formation which are both included in the model domain as is shown in Fig. 9. The caprock around the well is assumed to have been damaged, for example, during the drilling of the well or as a result of high pressures during injection. The damaged caprock is a leakage pathway for CO_2 from the storage reservoir. In the following, three simulations are shown which demonstrate the use of biofilms to reduce leakage from the reservoir.

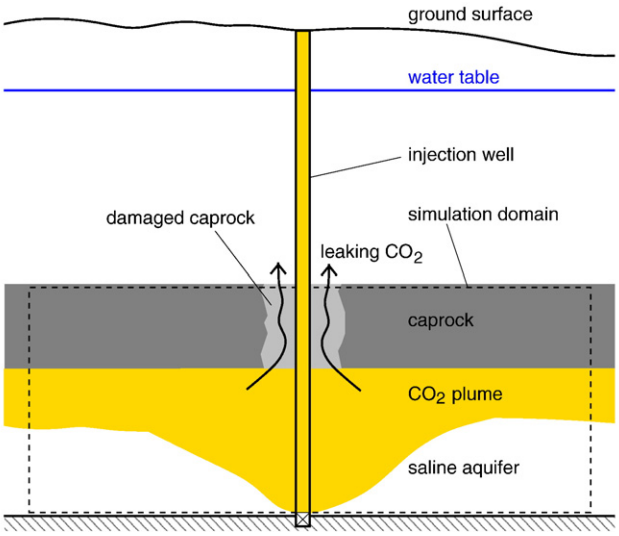


Fig. 9. Sketch of leakage scenario. The caprock near the injection well is damaged and serves as a leakage pathway for CO_2. The simulation domain comprises the caprock and the saline aquifer in which the CO_2 is stored.

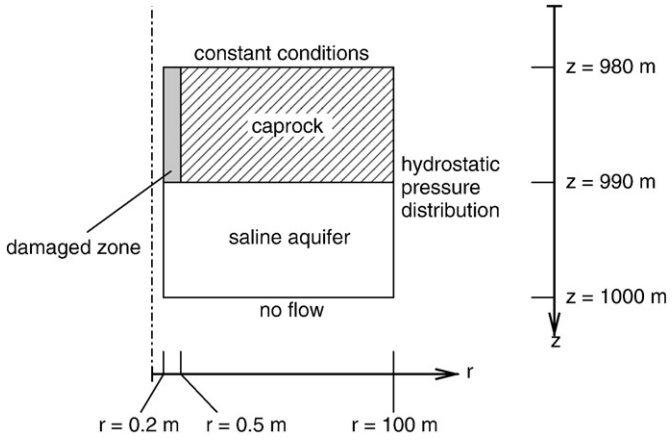


Fig. 10. Boundary conditions for the radially symmetric domain.

4.2. Description of model domain and simulation parameters

The model domain is radially symmetric, i.e., two-dimensional (r,z), with a radius of 100 m and a thickness of 20 m. The bottom of the domain is at 1000 m depth. As shown in Fig. 10, the caprock and the storage aquifer both have a thickness of 10 m, and the caprock is damaged up to a radius of 0.5 m. The simulation parameters including formation and fluid properties, and biological parameters are summarised in Table 8. The properties of brine are assumed to be constant, whereas those of CO_2 vary with pressure. Biomass attachment and detachment parameters $(c_{a,1}, c_{a,2}, c_{d,1}, \tilde{c}_{d,2})$ have been taken from the simulations in Section 3.1. Capillary pressure and relative permeabilities are calculated with the parameters given in Table 7 on page 29. Other parameters include the specific surface area of the rock formation $M = 2.2\times10^4\ \mathrm{m}^{-1}$, the diffusion coefficients $\hat{D}_p^b = \hat{D}_\kappa^s = 10^{-8}\ \mathrm{m}^2/\mathrm{s}$, and the effective diffusion coefficient $D_{eff}^s = \varepsilon\times10^{-9}\ \mathrm{m}^2/\mathrm{s}$.

Even though the model domain has a radius of 100 m, only the first 10 m are of interest and are finely meshed. This is done to capture relevant processes and strong gradients of the primary variables near the well. The mesh in the outer region ($r>10$ m) is very coarse (see Fig. 11) and only supposed to reduce the influence of the lateral boundary conditions, especially pressure, on the system. In vertical direction, the mesh is uniform with a size of 0.5 m, whereas in the horizontal direction, the element size varies between 0.2 m at the injection well and 42 m at the outer boundary.

Table 8
Simulation parameters.

Property/Parameter	Value	Comment
Formation properties and hydraulic properties of biofilm		
Aquifer permeability	$50\times10^{-15}\ \mathrm{m}^2$	
Aquifer porosity	0.22	
Aquifer thickness	10 m	
Caprock permeability	$1\times10^{-18}\ \mathrm{m}^2$	
Caprock porosity	0.22	
Caprock thickness	10 m	
Permeability of damaged zone	$20\times10^{-15}\ \mathrm{m}^2$	
Porosity of damaged zone	0.22	
Radius of damaged zone	0.5 m	
Permeability parameter $\phi_{p,c}/\phi_0$	0.35	
Permeability parameter n_k	3	From Table 7
Minimum permeability $K_{\min}$	$0.01\cdot K_0$	
Biofilm porosity ε	0.8	
Depth at bottom of aquifer	1000 m	
Injection well radius	0.2 m	
Domain radius	100 m	
Temperature T	40 °C	Isothermal
Fluid properties		
Brine salinity	0.15 kg/kg	
Brine density ϱ_w	1102 kg/m^3[a]	
Brine viscosity μ_w	9.63×10^{-4} Pa s[a]	
CO_2 density ϱ_n	$f(p,T)$[b]	
CO_2 viscosity μ_n	$f(p,T)$[c]	
Biological parameters		
Maximum substrate utilisation rate k_μ	$8.91\times10^{-5}\ \mathrm{s}^{-1}$	From Table 3
Monod half-saturation coefficient K_s	7.99×10^{-4} kg/m^3	
Yield coefficient Y	0.0975 kg/kg	
Endogenous decay rate b_0	$3.18\times10^{-7}\ \mathrm{s}^{-1}$	
Decay rate parameter c_c	$8.7\times10^{-4}\ \mathrm{s}^{-1}$	From Table 7
Decay rate parameter n_c	3	
Biofilm density ϱ_b	15 kg/m^3	

[a] [1].
[b] [45].
[c] [15].

4.3. Reference simulation: clogging of damaged caprock

This simulation shows the injection of bacteria and substrate into the formation and the subsequent injection of CO_2. The injected bacteria is expected to attach to the surface of the formation rock. Given the abundance of nutrients near the well, the bacteria can reproduce to form a biofilm occupying pore space and reducing the permeability of the formation rock, thus, preventing the CO_2 from leaking out of the formation.

4.3.1. Initial and boundary conditions

The formation is assumed to be initially filled with brine under hydrostatic conditions. It is also assumed that there is no biomass or substrate in the system. These conditions are assigned to the top and outer boundaries as constant boundary conditions. The bottom boundary is a no-flow boundary. The boundary conditions are shown in Fig. 10. The inner boundary, i.e., the injection well is also a no-flow boundary except at the interval over which water or CO_2 is being injected. Initially, water with suspended biomass is injected into the formation. This is followed by the injection of the nutrient medium containing the substrate. This, in turn, is followed by the injection of CO_2. The injection strategy is illustrated in Fig. 12. Different regions A,B,C, and D have been demarcated, each representing a different set of boundary conditions at the well as listed below. The total simulation time is 400 days.

A ($0\le t<0.167$ days; $989.25<z<994.75$ m)
- Water flow: 0.5 kg/s
- CO_2 flow: no flow
- Biomass flow: 4.54×10^{-7} kg/s. This corresponds to a biomass concentration in the injected medium of 10^{-3} kg/m^3.
- Substrate flow: no flow

B ($0.167\le t<90$ days; $989.25<z<994.75$ m)
- Water flow: 0.5 kg/s
- CO_2 flow: no flow
- Biomass flow: no flow
- Substrate flow (Continuum P): 1.13×10^{-4} kg/s. This corresponds to a substrate concentration in the injected medium of 0.25 kg/m^3.
- Substrate flow (Continuum F): no flow

C ($90\le t\le400$ days; $994.75<z\le1000$ m)
- Water flow: no flow
- CO_2 flow: 0.5 kg/s
- Biomass flow: no flow
- Substrate flow: no flow

D ($0\le t\le400$ days)
- No-flow conditions.

4.3.2. Results

The development of the biofilm in the vicinity of the injection well with time can be seen in Fig. 13. The figures show the biofilm volume

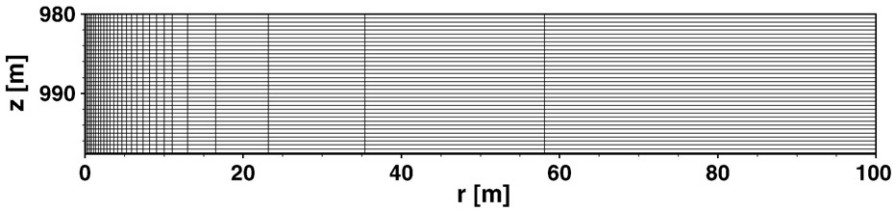


Fig. 11. Simulation mesh.

fraction ϕ_f/ε at six different times (10, 40, 90, 100, 140, and 400 days). The biofilm develops in the region into which the bacteria and substrate are injected. At $t = 90$ days, the injection of substrate is stopped and the injection of CO_2 starts, leading to a reduction of attached biomass with time. At the end of the simulation ($t = 400$ days), there is almost no biofilm left in the formation. The reduction of the amount of attached biomass is caused primarily by endogenous decay because the bacteria within the biofilm are protected from the supercritical CO_2. Suspended bacteria, however, are not protected from the biocidal effects of supercritical CO_2. That is why the concentration of suspended biomass in water drops strongly when CO_2 is injected into the formation as can be seen in Fig. 14. At $t = 100$ days, most of the suspended biomass has been damaged by CO_2.

Fig. 15 shows the total amount of attached and suspended biomass in the formation with respect to time. As substrate is injected, the biomass in the system increases steadily. When the injection of substrate is stopped, the amount of biomass reduces strongly. As mentioned earlier, this is as a result of the combination of endogenous decay and the biocidal effect of supercritical CO_2. However, one can see in the figure that the CO_2 kills almost all the suspended bacteria in a very short time, whereas the bacteria in the biofilm are – to an extent – protected from the CO_2.

The effect of the biofilm on the permeability of the formation can be seen in Fig. 16. The right column of figures shows the total permeability, i.e., the sum of the permeabilities of the two continua ($K = K_p + K_f$) at $t = 100, 140,$ and 400 days, and the left column shows the CO_2 saturation $S_{n,p}$ in Continuum P. The biofilm causes a considerable reduction of permeability preventing the CO_2, which is injected below the biofilm, from leaking through the damaged zone. However, as biomass decay within the biofilm progresses, the permeability increases. At $t = 400$ days, no influence of attached biomass on the permeability can be seen. This would mean that a renewal of the biofilm by the injection of nutrients would be necessary at some point. A more lasting solution would be the use of biofilms which actively precipitate $CaCO_3$ minerals as mentioned in Section 1.2.

In Section 4.4, a renewal of the substrate at regular intervals even during CO_2 injection is modelled. Even though the model does not account for mineral precipitation, Section 4.5 studies the implications

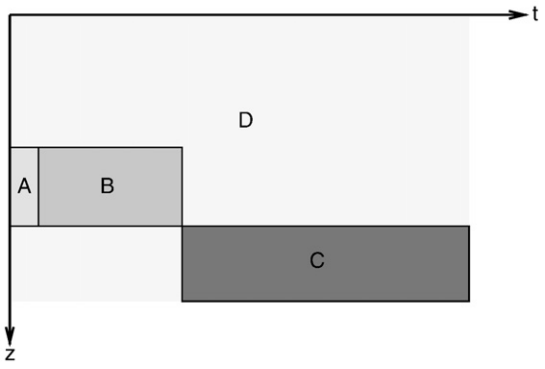


Fig. 12. Reference simulation: boundary conditions at the well.

a biobarrier consisting of biofilm and mineral precipitates would have on the system by using a reduced biofilm decay rate.

4.4. Variation 1: continued injection of substrate medium

In this simulation, all the parameters, mesh, domain etc. are exactly the same as in the reference simulation. Only the boundary conditions at the injection well differ from those of the reference simulation. These are illustrated in Fig. 17a. The injection well is divided into different regions (A, B, C, D, E) in space z and time t. The regions A, B, C, and D are identical to those of the reference simulation.

E represents the injection of substrate at intervals and is simultaneous to C (the injection of CO_2). The boundary conditions in E are defined below.

E $(90 \leq t \leq 400$ days; $989.25 < z \leq 994.75$ m)

- Water flow: $f_e(t) \cdot 0.5$ kg/s
- CO_2 flow: no flow
- Biomass flow: no flow
- Substrate flow (Continuum P): $f_e(t) \cdot 1.13 \times 10^{-4}$ kg/s. This corresponds to a substrate concentration in the injected medium of 0.25 kg/m^3.
- Substrate flow (Continuum F): no flow

$f_e(t)$ is the positive part of a sine function of time with a period T of 120 days and a unit amplitude as defined in Eq. (42).

$$f_e(t) = max\left(0, -sin\left(\frac{t - t_0}{T / 2\pi}\right)\right), \tag{41}$$

where $t_0 = 90$ days marks the beginning of region E. A plot of the resulting mass flow of water over the boundary of the injection well for the regions A, B, and E is given in Fig. 17b.

4.4.1. Results

Fig. 18a shows the total amount of biomass in the formation over time. As is the case in the reference simulation, there is a build-up of attached and suspended biomass in the formation during the first 90 days. This is followed by a strong drop when the substrate injection is stopped and CO_2 is injected. However, in contrast to the reference simulation, the amount of biomass in the system increases again when the injection of the nutrient medium is resumed. There is a cyclic pattern corresponding to the injection strategy as shown in Fig. 17 b. One can see that the amount of suspended biomass reduces very quickly when the medium injection is shut down compared to that of the attached biomass.

The CO_2 saturation and the total permeability of the formation at three time-steps, i.e., at 180, 270, and 400 days are shown in Fig. 19. The magnitude and extent of permeability reduction changes with time. They are greatest in the middle of an injection phase, e.g., at $t = 180$ days and lowest at the end of a starvation phase, e.g., at $t = 270$ days.

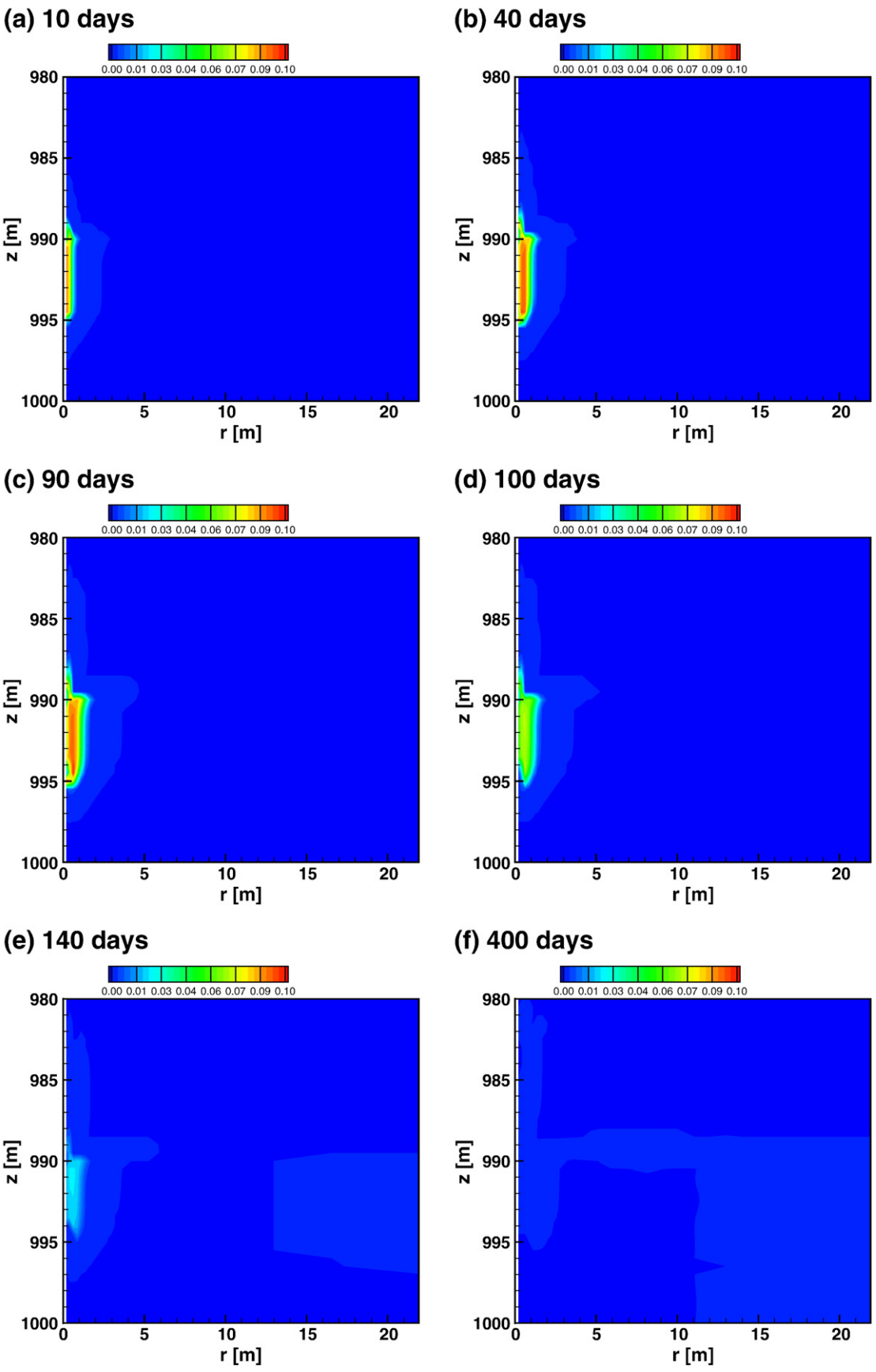


Fig. 13. Results of reference simulation: volume fraction of space occupied by biofilm ϕ_f/ε.

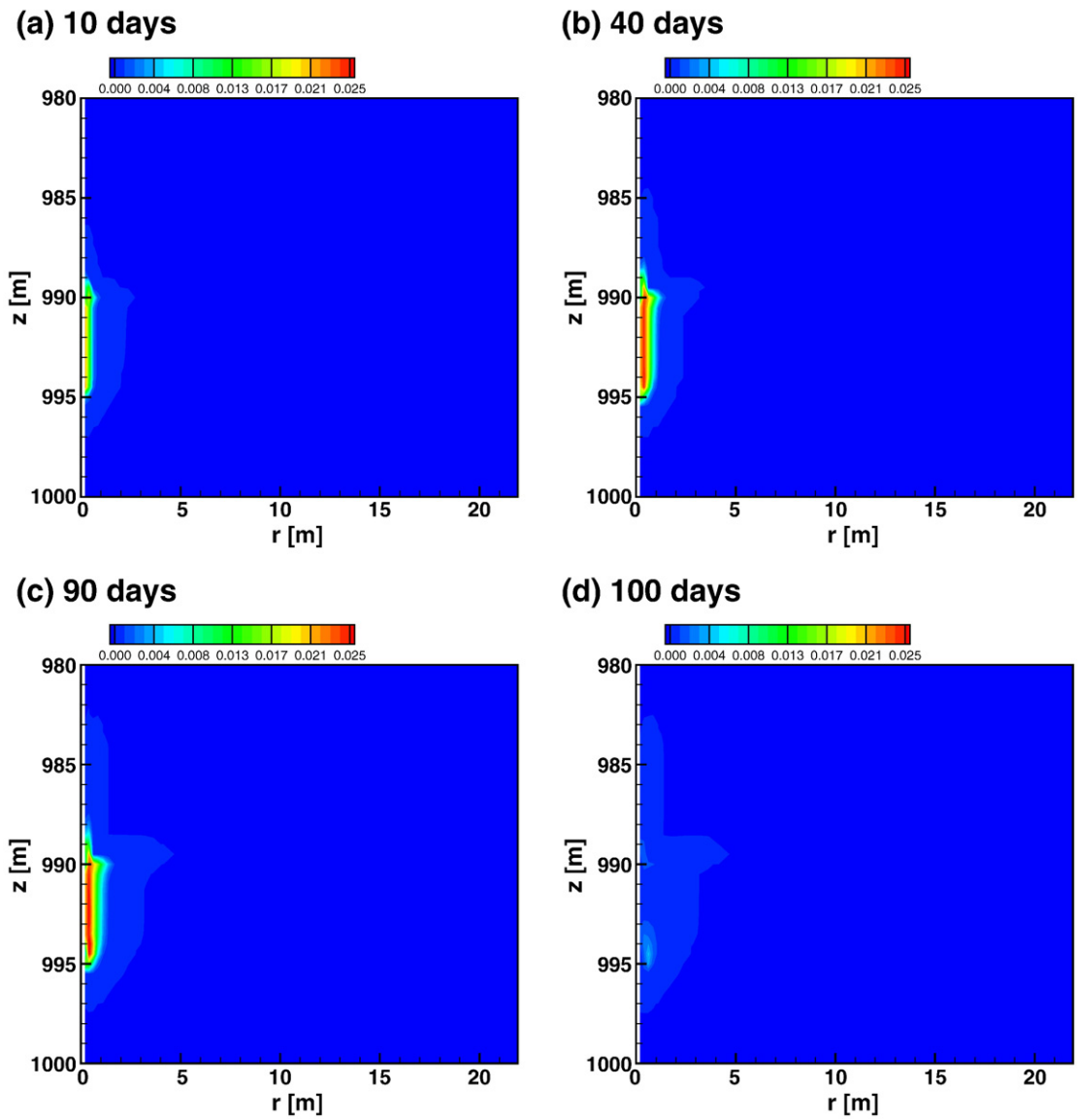


Fig. 14. Results of reference simulation: concentration of suspended biomass in water C_w^b.

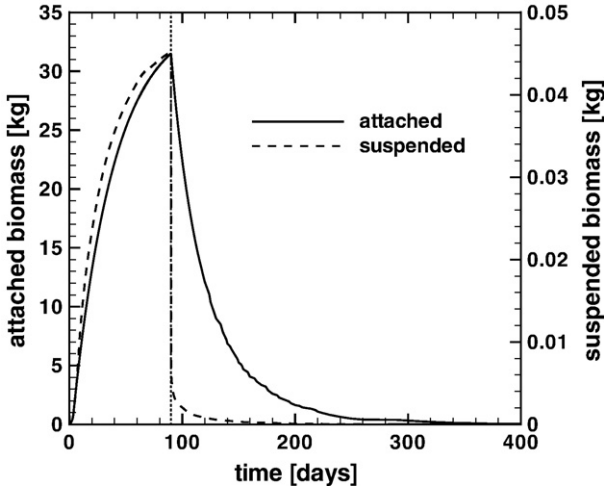


Fig. 15. Reference simulation: amount of biomass (attached and suspended) in the formation. The dotted vertical line at $t = 90$ days marks the end of substrate injection and the start of CO_2 injection. Note that the amount of suspended biomass is about two orders of magnitude less than that of the attached biomass.

4.5. Variation 2: reduced biofilm decay rate

One way of increasing the durability of the biobarrier is to use biofilms which mediate the precipitation of $CaCO_3$, thus forming a biobarrier which consists of biofilm and mineral precipitates [12]. This process cannot be modelled explicitely here. But, the potential effect it would have on the system is studied in this variation of the reference simulation. This is done by assuming that a biomineral barrier has been formed in the same places as in the reference simulation, and that this biomineral barrier has a decay rate which is two orders of magnitude less than in the reference case, i.e.,

$$b_f = 0.01 \cdot \left(3.18 \times 10^{-7} + 8.7 \times 10^{-4} \cdot S_{n,f}^3\right) s^{-1}. \quad (42)$$

This is an arbitrary choice. However, recent experiments on this topic at the Center for Biofilm Engineering, Montana State University, suggest that decay of biomineral deposits is very slow, although an exact quantification is not available yet.

The simulation starts at $t = 90$ days, and the initial conditions here are the conditions in the reference simulation at $t = 90$ days. The boundary conditions and all other parameters remain unchanged.

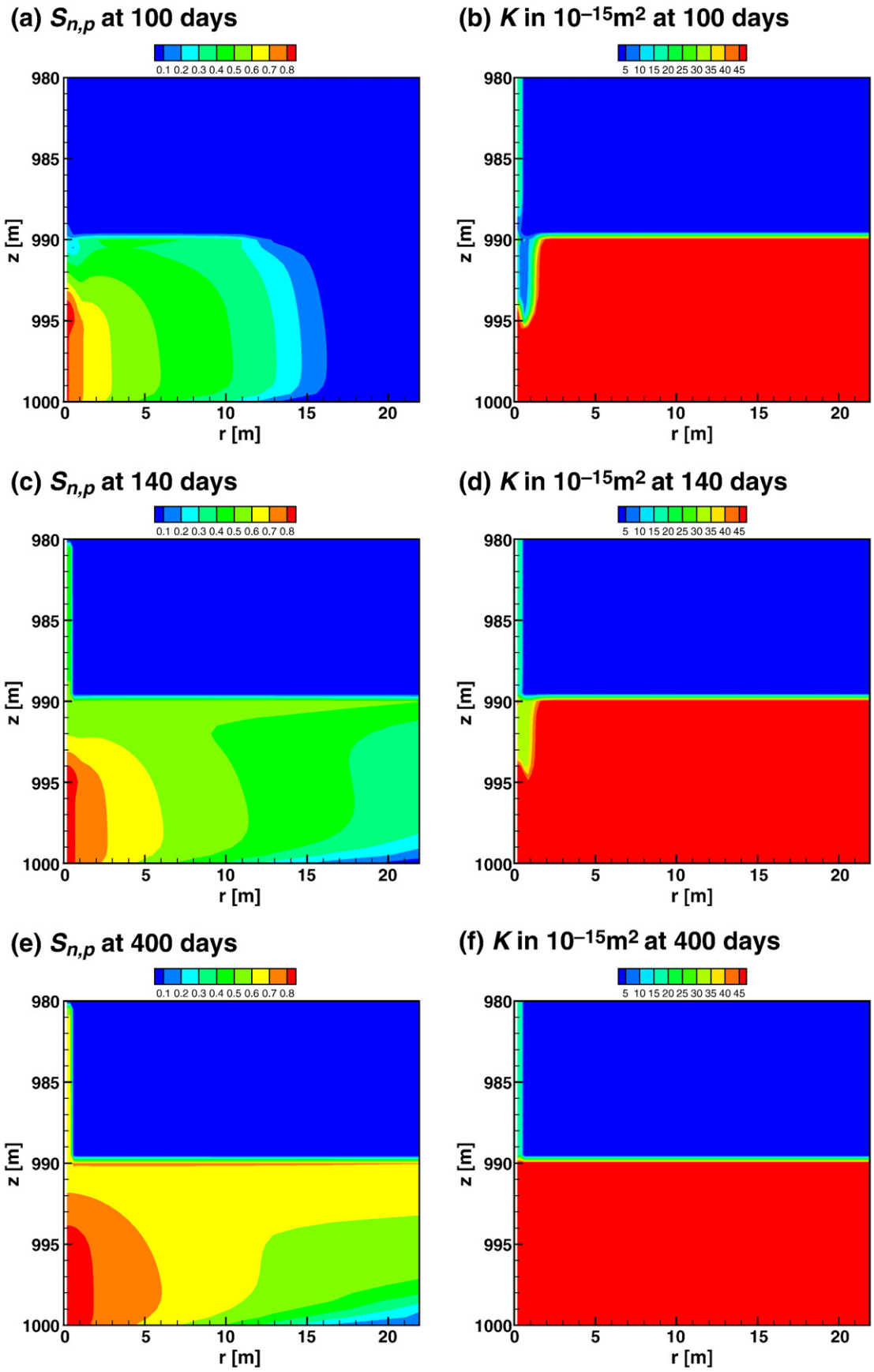


Fig. 16. Results of reference simulation: $S_{n,p}$ (left) and $K = K_p + K_f$ (right).

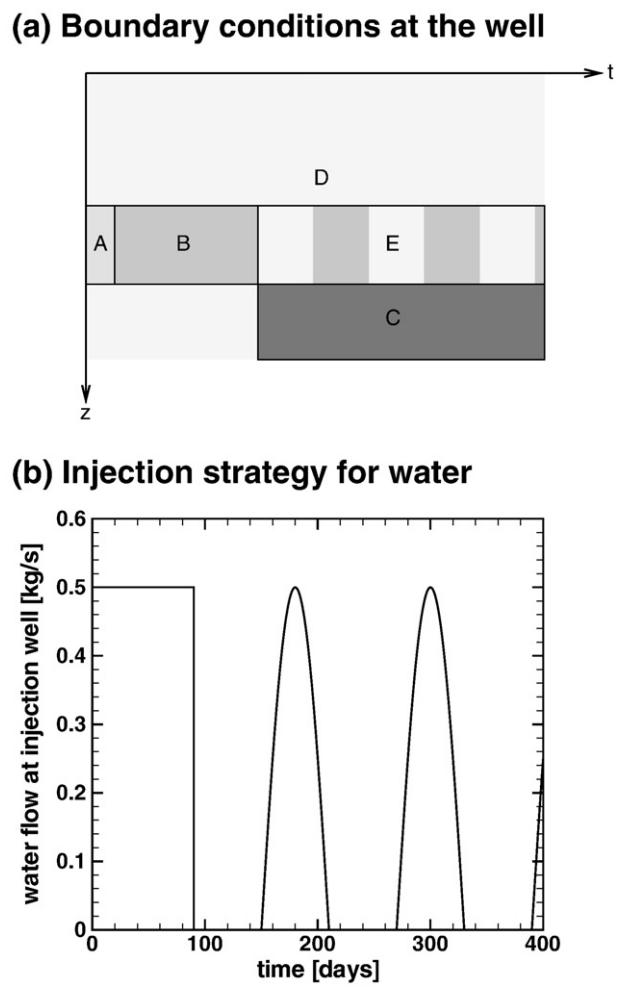


Fig. 17. Variation 1: water is injected initially at a constant rate of 0.5 kg/s (A and B). As from 90 days (E), the injection rate is a function of time.

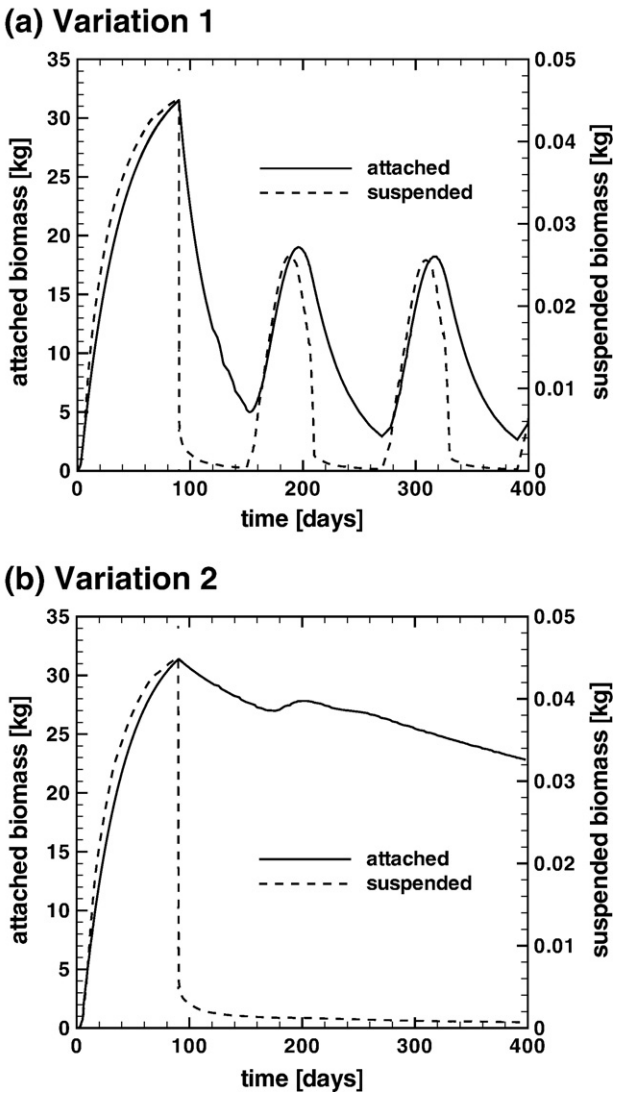


Fig. 18. Variations: amount of biomass (attached and suspended) in the formation.

4.5.1. Results

The results in Fig. 18b, i.e., the total biomass in the system over time, show that the amount of suspended biomass is the same as in the reference simulation. The amount of attached "biomass" (which is composed of biofilm and biominerals) does not drop as quickly as in the reference case. This is obviously due to the reduced biofilm decay rate. There is a slight increase in attached biomass at about $t = 190$ days. This occurs when biofilm growth, which still occurs as long as the injected substrate has not been fully consumed, exceeds biofilm decay in total.

4.6. Remarks

The simulations show that the presented model is capable of qualitatively modelling the accumulation of biomass in a geological formation in the presence of water and CO_2 as well as the effects of the accumulated biomass on the hydraulic properties of the formation. In the simulations, the bacterial cells embedded in the biofilm are protected from supercritical CO_2, and thus the biofilm persists longer than the suspended cells. The biofilm can even grow in the presence of CO_2 when nutrients are injected. These are important prerequisites for the use of biofilms to increase storage safety. However, in the presence of supercritical CO_2, an important process which enhances the spreading of the biofilm is strongly inhibited, i.e., the transport of detached cells and subsequent reattachment at new sites. Since detached cells leave the protective environment of the biofilm, the presence of a biocide in the bulk fluid prevents them from successfully colonising new surfaces.

5. Summary and conclusions

This article deals primarily with the development of a numerical model capable of describing the accumulation of biomass in the subsurface and its application to the plugging of damaged caprock in a subsurface CO_22 storage reservoir. This involves the description of fluid flow and microbial activity in porous media. On the one hand, the accumulation of biomass in a porous medium changes the hydraulic properties of the medium which affects flow. Flow processes, on the other hand, determine the transport of nutrients to the microbes, and thus directly influence the rate and distribution of biomass growth. Thus, the proper description of the interaction between flow and microbial processes is an essential challenge for such a model.

Two sets of experiments with particular relevance to the processes of interest were chosen for the validation of the model. By comparison of simulation results to the results of one of the experiments, which considers one-phase flow through a sand column, it could be shown that the model can qualitatively reproduce and predict the relevant processes for the given conditions. However, quantitative validation was not possible. Due to lack of information and the complexity of the system, the second set of experiments could not be used for validation purposes. Rather, it served as a source of calibration for the model.

Finally, the model was applied to a fictitious test scenario in which the caprock of a CO_2 storage reservoir is damaged at the injection well.

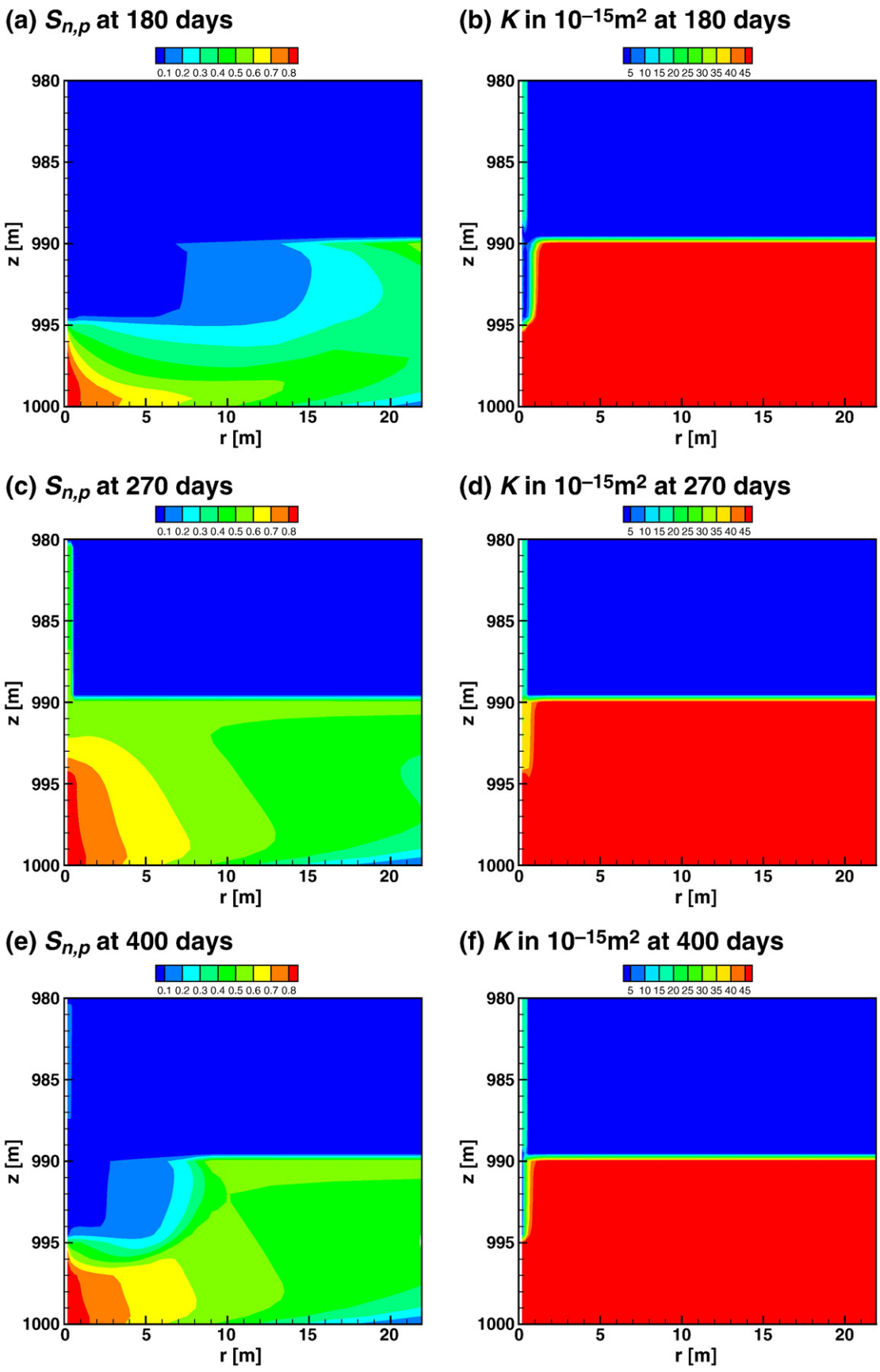


Fig. 19. Results of variation 1: $S_{n,p}$ (left) and $K = K_p + K_f$ (right).

Bacterial cells and nutrients are injected into the formation just below the caprock until a biofilm is formed within the damaged zone. CO_2 is then injected into the formation. For the given example, it is possible to plug the damaged caprock with biofilm. However, the biofilm is temporary and requires regular feeding. This problem could be solved by the use of biofilms which serve as catalysts for the precipitation of minerals, leading to longer-lasting clogging. The described model does not account for geochemical processes, and such scenarios cannot be modelled yet. Thus, in future work, an extension of the model to account for such processes is important. If it is possible to transport the chemical species necessary for biomineralisation to the biofilm, the use of this technology to plug leakage pathways can be a very useful method of mitigating leakage and increasing storage safety.

6. Outlook

The capabilities of the model allow the simulation of biofilm formation in the subsurface. However, there is very much room for improvement. Further work on this topic should include the following points.

- Some of the simplifications made in the development of the model are restrictive and need to be revisited. A good example is the assumption that both continua have the same pressure. This way, the advective exchange of solutes between the two continua cannot be accounted for. Instead, both pressures could be solved for independently and linked only with the exchange term. The exchange of solutes would then be driven by a combination of solute and pressure gradients.
- Dissolved CO_2 plays an important role in the inactivation of bacterial cells [65]. Thus, an extension of the model to account for the dissolution of CO_2 in water and its subsequent transport within the water phase is necessary and would improve the capability of the model to capture the biocidal effect of CO_2 on the microorganisms, especially the suspended cells.
- The model assumes that there is only one growth-limiting substrate and that all other nutrients necessary for growth are abundantly available. This is a strong restriction. An injection strategy could involve the injection of a substrate and the delayed injection of an electron acceptor with the aim of growing a biofilm at some distance from the injection. This cannot be simulated with the model. Thus, an electron acceptor needs to be accounted for by the model.
- The model makes use of many empirical parameters and relationships. Sensitivity studies are necessary to determine the parameters which have the strongest influence on the system. Values for these parameters need to be determined in experimental investigations. Experiments are also necessary to gain a better understanding of the relevant mechanisms involved.
- All the equations, correlations, and parameters used in the model are defined on the macroscale. However, it is often easier to understand and describe processes on the microscale. Well-understood microscale phenomena should be properly depicted on the macroscale. This is not always easy. Therefore, research on the upscaling of microscale processes relevant to biofilms in porous media to the macroscale (e.g., [19,56]) is absolutely necessary.
- The conservation equations of the different components (water, CO_2, biomass, and substrate) are solved simultaneously. This is computationally expensive. Future work could focus on decoupling processes of different time scales. For example, the simulation of flow processes, involving water and CO_2, could be partly decoupled from transport and biological processes, involving biomass and substrate.
- Under starvation conditions, the biobarrier slowly loses its efficiency. A more enduring option is the use of mineral-precipitating biofilms. In further work, it could be of interest to extend the model to account for the transport of the chemical species necessary for such mineralisation.

Acknowledgement

This work was carried out within the framework of the International Research Training Group NUPUS (http://www.nupus.uni-stuttgart.de) funded by the German Research Foundation DFG (GRK 1398) and the Netherlands Organisation for Scientific Research NWO (DN 81-754). The authors acknowledge support by the US Department of Energy Zero Emissions Research and Technology (ZERT) programme (DOE Award No. DE-FC26-04NT42262) and from the US Department of Energy EPSCoR programme under grant number DE-FG02-08ER46527.

Appendix A. Notation

Symbol	Definition	Dimension
ε	Biofilm porosity	[–]
ϕ	Porosity	[–]
ϕ_0	Porosity of porous medium unaffected by biofilm	[–]
$\phi_{p,c}, \phi'_{p,c}$	Parameters for the calculation of K_p and K_f	
λ	Pore-size distribution index	[–]
μ_α	Dynamic fluid viscosity of the phase α	[kg/(m s)]
μ_κ	Growth rate of biomass in Continuum κ	[1/s]
ϱ_α	Fluid density of the phase α	[kg/m^3]
ϱ_b	Biofilm density	[kg/m^3]
C_w^b	Concentration of biomass in water	[kg/m^3]
C_w^s	Concentration of substrate in water	[kg/m^3]
D	Diffusion coefficient	[m^2/s]
F	Continuum accounting for fluid flow in biofilm	
P	Continuum accounting for fluid flow in porous matrix	
K	Isotropic intrinsic permeability	[m^2]
K_0	Permeability of biofilm-free porous medium	[m^2]
$K_{\min}$	Permeability of biofilm-filled porous medium	[m^2]
K_s	Monod half-saturation coefficient	[kg/m^3]
M	Specific surface	[m^2/m^3]
S	Saturation	[–]
S_r	Residual saturation	[–]
S_e	Effective saturation	[–]
T	Temperature	[°C]
Y	Yield coefficient	
a	Exchange parameter	[s/m^2]
b	Biomass decay rate	[1/s]
b_0	Endogenous biomass decay rate	[1/s]
b_c	Biomass decay rate due to lysis	[1/s]
c_c	Parameter for the calculation of b_c	
$c_{a,1}, c_{a,2}$	Parameters for the calculation of k_a	
$c_{d,1}, c_{d,2}, \tilde{c}_{d,2}$	Parameters for the calculation of k_d	
d_r	Characteristic pore diameter	[m]
e	Exchange term	[kg/(m^{3}s)]
$\mathbf{g}$	Vector of gravitational acceleration $(0,0,-g)^T$	[m/s^2]
g	(Scalar) gravitational acceleration	[m/s^2]
k_μ	Maximum substrate utilisation rate	[1/s]
k_a	Attachment function	[1/s]
k_d	Detachment function	[1/s]
k_d^τ	Detachment due to shear	[1/s]
k_d^d	Detachment due to biological factors	[1/s]
k_r	Relative permeability	[–]
n_c	Parameter for the calculation of b_c	
n_k	Parameters for the calculation of K_p	
p	Pressure	[N/m^2]
p_d	Entry pressure	[N/m^2]
p_c	Capillary pressure	[N/m^2]
q	Source/sink	[kg/(m^{3}s)]
r_g	Biomass growth	[kg/(m^{3}s)]
r_b	Biomass decay	[kg/(m^{3}s)]
r_a	Biomass attachment rate	[kg/(m^{3}s)]
r_d	Biomass detachment rate	[kg/(m^{3}s)]
$\mathbf{v}$	Darcy flux/velocity	[m/s]

Subscripts		*Superscripts*	
α	Phase, either w or n	b	Biomass
n	Non-wetting phase	s	Substrate/solute
w	Wetting phase		
κ	Continuum, either p or f		
p	Continuum P		
f	Continuum F		

References

[1] Batzle M, Wang ZJ. Seismic properties of pore fluids. Geophysics Nov. 1992;57 (11):1396–408.
[2] Bear J. Hydraulics of Groundwater. McGraw-Hill; 1979.
[3] Bryers JD. Biofilms II: Process Analysis and Applications. Ch. 1.1 Biofilms: An Introduction. Wiley; 2000. p. 3–12.
[4] Cary JW. Estimating the surface-area of fluid-phase interfaces in porous-media. J Contam Hydrol 1994;15(4):243–8.
[5] Chen-Charpentier B. Numerical simulation of biofilm growth in porous media. J Comput Appl Math 1999;103(1):55–66.
[6] Clement TP, Hooker BS, Skeen RS. Macroscopic models for predicting changes in saturated porous media properties caused by microbial growth. Ground Water 1996;34(5):934–42.
[7] Clement TP, Peyton BM, Ginn TR, Skeen RS. Modeling bacterial transport and accumulation processes in saturated porous media: a review. Adv Nucl Sci Technol 1999;26:59–78.
[8] Cooke AJ, Rowe RK, Rittmann BE. Modelling species fate and porous media effects for landfill leachate flow. Can Geotech J 2005;42(4):1116–32.
[9] Corapcioglu MY, Haridas A. Transport and fate of microorganisms in porous media: a theoretical investigation. J Hydrol 1984;72(1–2):149–69.
[10] Corey AT. Mechanics of Immiscible Fluids in Porous media. Water Resources Publications; 1994.
[11] Cunningham AB, Characklis WG, Abedeen F, Crawford D. Influence of biofilm accumulation on porous media hydrodynamics. Environ Sci Technol 1991;25(7): 1305–11.
[12] Cunningham AB, Gerlach R, Spangler L, Mitchell AC. Microbially enhanced geologic containment of sequestered supercritical CO_2. Energy Procedia 2009;1 (1):3245–52 Feb.
[13] De Beer D, Stoodley P, Lewandowski Z. Liquid flow in heterogeneous biofilms. Biotechnol Bioeng 1994;44(5):636–41 Aug.
[14] Ebigbo A, Class H, Helmig R. CO_2 leakage through an abandoned well: problem-oriented benchmarks. Comput Geosci 2007;11(2):103–15.
[15] Fenghour A, Wakeham WA, Vesovic V. The viscosity of carbon dioxide. J Phys Chem Ref Data 1998;27(1):31–44.
[16] Foppen JW, Van Herwerden M, Schijven J. Measuring and modelling straining of *Escherichia coli* in saturated porous media. J Contam Hydrol 2007;93(1–4):236–54.
[17] Gargiulo G, Bradford S, Simunek J, Ustohal P, Vereecken H, Klumpp E. Bacteria transport and deposition under unsaturated conditions: the role of the matrix grain size and the bacteria surface protein. J Contam Hydrol 2007;92(3–4):255–73.
[18] Gerke HH, van Genuchten MT. Macroscopic representation of structural geometry for simulating water and solute movement in dual-porosity media. Adv Water Resour 1996;19(6):343–57 Dec.
[19] Golfier F, Wood BD, Orgogozo L, Quintard M, Buès M. Biofilms in porous media: development of macroscopic transport equations via volume averaging with closure for local mass equilibrium conditions. Adv Water Resour 2009;32:463–85.
[20] Ham YJ, Kim SB, Park SJ. Numerical experiments for bioclogging in porous media. Environ Technol 2007;28(10):1079–89.
[21] Helmig R. Multiphase Flow and Transport Processes in the Subsurface. Springer; 1997.
[22] Hornberger GM, Mills AL, Herman JS. Bacterial transport in porous media: evaluation of a model using laboratory experiments. Water Resour Res 1992;28 (3):915–38.
[23] Kapellos GE, Alexiou TS, Payatakes AC. Hierarchical simulator of biofilm growth and dynamics in granular porous materials. Adv Water Resour 2007;30(6–7): 1648–67.
[24] Kim SB. Numerical analysis of bacterial transport in saturated porous media. Hydrol Process 2006;20(5):1177–86.
[25] Kopp, A., Binning, P. J., Johannsen, K., Class, H., Helmig, R. A Contribution to Risk Analysis for Leakage through Abandoned Wells in Geological CO_2 Storage. Submitted to Advances in Water Resources submitted for publication.
[26] Kopp A, Ebigbo A, Bielinski A, Class H, Helmig R. Numerical simulation of temperature changes caused by CO_2 injection in geological reservoirs. In: Grobe M, Pashin JC, Dodge RL, editors. Carbon dioxide sequestration in gelogical media–State of the science. Vol. 59 of AAPG Studies in Geology. Ch. 26; 2009. p. 439–56.
[27] Korteland S, Bottero S, Hassanizadeh S, Berentsen C. What is the correct definition of average pressure? Transp Porous Med 2009, doi:10.1007/s11242-009-9490-2.
[28] Maggi F, Porporato A. Coupled moisture and microbial dynamics in unsaturated soils. Water Resour Res 2007;43(7):W07444.
[29] Mitchell AC, Phillips AJ, Hamilton MA, Gerlach R, Hollis WK, Kaszuba JP, et al. Resilience of planktonic and biofilm cultures to supercritical CO_2. J Supercrit Fluids 2008;47(2):318–25 Dec.
[30] Mitchell AC, Phillips AJ, Hiebert R, Gerlach R, Spangler LH, Cunningham AB. Biofilm enhanced geologic sequestration of supercritical CO_2. Int J Greenhouse Gas Control 2009;3(1):90–9 Jan.
[31] Mostafa M, Van Geel PJ. Conceptual models and simulations for biological clogging in unsaturated soils. Vadose Zone J 2007;6(1):175–85.
[32] Murphy EM, Ginn TR. Modeling microbial processes in porous media. Hydrogeol J 2000;8(1):142–58.
[33] Niemet MR, Rockhold ML, Weisbrod N, Selker JS. Relationships between gas–liquid interfacial surface area, liquid saturation, and light transmission in variably saturated porous media. Water Resour Res 2002;38(8):1135.
[34] Nordbotten JM, Celia MA, Bachu S, Dahle HK. Semi-analytical solution for CO_2 leakage through an abandoned well. Environ Sci Technol 2005;39(2):602–11.
[35] Oldenburg CM. Screening and ranking framework for geologic CO_2 storage site selection on the basis of health, safety, and environmental risk. Environ Geol 2008;54(8):1687–94 Jun.
[36] Picioreanu C, van Loosdrecht MCM, Heijnen JJ. Two-dimensional model of biofilm detachment caused by internal stress from liquid flow. Biotechnol Bioeng 2001;72 (2):205–18.
[37] Pruess K. Thermal Effects During CO_2 Leakage from a Geologic Storage Reservoir. Tech. Rep. LBNL-55913. Lawrence Berkeley National Laboratory; 2004.
[38] Pruess K. Numerical studies of fluid leakage from a geologic disposal reservoir for co_2 show self-limiting feedback between fluid flow and heat transfer. Geophys Res Lett 2005;32(14):L14404 Jul.
[39] Rittmann BE. The effect of shear stress on biofilm loss rate. Biotechnol Bioeng 1982;24(2):501–6.
[40] Rittmann BE. The significance of biofilms in porous media. Water Resour Res 1993;29:2195–202.
[41] Rockhold ML, Yarwood RR, Niemet MR, Bottomley PJ, Selker JS. Considerations for modeling bacterial-induced changes in hydraulic properties of variably saturated porous media. Adv Water Resour 2002;25(5):477–95.
[42] Rockhold ML, Yarwood RR, Selker JS. Coupled microbial and transport processes in soils. Vadose Zone J 2004;3(2):368–83.
[43] Schaefer A, Ustohal P, Harms H, Stauffer F, Dracos T, Zehnder AJB. Transport of bacteria in unsaturated porous media. J Contam Hydrol 1998;33(1–2):149–69.
[44] Seki K, Miyazaki T. A mathematical model for biological clogging of uniform porous media. Water Resour Res 2001;37(12):2995–9.
[45] Span R, Wagner W. A new equation of state for carbon dioxide covering the fluid region from the triple-point temperature to 1100 K at pressures up to 800 MPa. J Phys Chem Ref Data 1996;25(6):1509–96.
[46] Speitel GE, DiGiano FA. Biofilm shearing under dynamic conditions. J Environ Eng-Asce 1987;113(3):464–75 Jun.
[47] Stewart PS. A review of experimental measurements of effective diffusive permeabilities and effective diffusion coefficients in biofilms. Biotechnol Bioeng 1998;59(3):261–72 Aug.
[48] Stoodley P, De Beer D, Lewandowski Z. Liquid flow in biofilm systems. Appl Environ Microbiol 1994;60(8):2711–6 Aug.
[49] Tan Y, Gannon JT, Baveye P, Alexander M. Transport of bacteria in an aquifer sand: experiments and model simulations. Water Resour Res 1994;30(12):3243–52.
[50] Taylor SW, Jaffé PR. Biofilm growth and the related changes in the physical properties of a porous medium 1. Experimental investigation. Water Resour Res 1990;26(9):2153–9.
[51] Taylor SW, Jaffé PR. Substrate and biomass transport in a porous medium. Water Resour Res 1990;26(9):2181–94.
[52] Taylor SW, Milly PCD, Jaffé PR. Biofilm growth and the related changes in the physical properties of a porous medium 2. Permeability. Water Resour Res 1990;26(9):2161–9.
[53] Thullner M, Schroth MH, Zeyer J, Kinzelbach W. Modeling of a microbial growth experiment with bioclogging in a two-dimensional saturated porous media flow field. J Contam Hydrol 2004;70(1–2):37–62.
[54] Thullner M, Zeyer J, Kinzelbach W. Influence of microbial growth on hydraulic properties of pore networks. Transp Porous Med 2002;49(1):99–122.
[55] van Loosdrecht MCM, Lyklema J, Norde W, Zehnder AJ. Influence of interfaces on microbial activity. Microbiol Mol Biol Rev 1990;54(1):75–87.
[56] van Noorden TL, Pop IS, Ebigbo A, Helmig R. An upscaled model for biofim growth in a thin strip. Water Resources Research 2010, doi:10.1029/2009WR008217.
[57] Vandevivere P. Bacterial clogging of porous-media—a new modeling approach. Biofouling 1995;8(4):281–91.
[58] Vandevivere P, Baveye P. Effect of bacterial extracellular polymers on the saturated hydraulic conductivity of sand columns. Appl Environ Microbiol 1992;58(5):1690–8.
[59] Wan JM, Wilson JL, Kieft TL. Influence of the gas–water interface on transport of microorganisms through unsaturated porous-media. Appl Environ Microbiol 1994;60(2):509–16.
[60] Wood BD, Ford RM. Biological processes in porous media: from the pore scale to the field. Adv Water Resour 2007;30(6–7):1387–91.
[61] Wood BD, Quintard M, Whitaker S. Calculation of effective diffusivities for biofilms and tissues. Biotechnol Bioeng 2002;77(5):495–516 Mar.
[62] Xu TF, Ontoy Y, Molling P, Spycher N, Parini M, Pruess K, et al. Reactive transport modeling of injection well scaling and acidizing at Tiwi field, Philippines. Geothermics 2004;33(4):477–91 Aug.
[63] Yarwood RR, Rockhold ML, Niemet MR, Selker JS, Bottomley PJ. Impact of microbial growth on water flow and solute transport in unsaturated porous media. Water Resour Res 2006;42:W10405.
[64] Zekri AY. Microbial enhanced oil recovery—a short review. Oil Gas Eur Mag 2001;1:22–5.
[65] Zhang J, Davis TA, Matthews MA, Drews MJ, LaBerge M, An YH. Sterilization using high-pressure carbon dioxide. J Supercrit Fluids 2006;38(3):354–72 Oct.
[66] Zhang TC, Bishop PL. Density, porosity, and pore structure of biofilms. Water Res 1994;28(11):2267–77.